Model-Based Study of Near-Surface Transport in and around Cape Cod Bay, Its Seasonal Variability, and Response to Wind

MARGARET GREGORY,[a] IRINA I. RYPINA,[b] SACHIKO YOSHIDA,[c] AND ALISON M. MACDONALD[b]

[a] *The MIT-WHOI Joint Program in Oceanography/Applied Ocean Science and Engineering, Woods Hole, Massachusetts*
[b] *Physical Oceanography Department, Woods Hole Oceanographic Institution, Woods Hole, Massachusetts*
[c] *Department of Oceanograhpy, University of Hawai'i at Manoa, Honolulu, Hawaii*

(Manuscript received 6 February 2024, in final form 17 July 2024, accepted 3 October 2024)

ABSTRACT: Output from a high-resolution numerical model is used to study near-surface transport in and around Cape Cod Bay using a Lagrangian approach. Key questions include the following: What are the dominant transport pathways? How do they vary in time on seasonal-to-interannual scales? What is the role of wind in driving this variability? Application to a possible release of wastewater into Cape Cod Bay from the recently closed Pilgrim Nuclear Power Station is discussed. Analysis reveals a seasonality in Cape Cod Bay transport patterns, with shorter residence times throughout the bay and an increased probability of outflow waters exiting the bay during spring and summer. Wind-induced Ekman currents are identified as a dominant driver of this variability.

SIGNIFICANCE STATEMENT: This study is motivated by a possible release of radioisotope-contaminated wastewater into Cape Cod Bay, a region important to fishing, aquaculture, and tourist industries. The specific aim is to better understand near-surface transport patterns and mechanisms in Cape Cod Bay both in general and within the context of a wastewater release from Pilgrim Nuclear Power Station.

KEYWORDS: Coastal flows; Lagrangian circulation/transport; Regional models

1. Introduction

In 2019, Pilgrim Nuclear Power Station (PNPS), located on the coast of Plymouth, Massachusetts, was closed and sold to Holtec International to be decommissioned. As part of the decommissioning process, four million liters of stored radioactive wastewater used to cool the reactor must be disposed of (Fraser 2022). At the time of writing this paper, four disposal methods have been proposed: evaporating the water, storing the wastewater on site and waiting for the radionuclides to decay, transporting the water to a long-term storage facility, or releasing the wastewater off the coast of PNPS into Cape Cod Bay (Holtec International 2022, 2023). The potential release of wastewater into the bay could have notable local environmental impacts affecting fisheries, aquaculture, and, possibly, the general population. This study and a previous study by Rypina et al. (2022) were largely motivated by concerns voiced by the local community and the state of Massachusetts. Motivated by a potential wastewater release from PNPS, Rypina et al. (2022) used drifter data to identify two likely spreading pathways of the plume: one from PNPS toward the eastern elbow of the bay and another extending from PNPS, past Race Point, and out of the bay. With only 417 drifters available, however, Rypina et al. (2022) were not able to study seasonal or interannual variability in the transport, its response to wind, or the circulation pattern's small-scale features. Here, we present a more in-depth study of the transport within Cape Cod Bay and utilize time-evolving, high-resolution model output which has the temporal resolution required to resolve seasonal variability. The model output also allows investigation of the dominant physical drivers of transport and exchange. In addition to considering the fate of a potential PNPS wastewater release, we also extend the methods to characterize the transport of particles released throughout the entire bay. Here we use the terms particles and particle trajectories to denote infinitesimal water parcels and their model-simulated pathways.

To that end, our first goal is to determine the temporal variability of the probable spreading pathways of a potential wastewater plume and the timing of spreading within and out of Cape Cod Bay. Using velocity fields obtained from the Gulf of Maine Operational Forecast System (GoMOFS), a high-resolution model that allows detailed study of the region's dynamics including seasonal and interannual variability, large ensembles of simulated trajectories were estimated for particles released off PNPS to investigate the spreading from a Lagrangian viewpoint. In general, wastewater from nuclear power plants contains both radionuclides that are heavier than water and will sink or that are water soluble (Buesseler 2020). The former would have to be considered separately as they cannot be modeled as following the currents and are not the subject of this study. The soluble radionuclides, such as tritium, serve as passive tracers and can be modeled as water flow. We investigated surface flow in this study (assuming small vertical velocities) as a first approximation of the movement of soluble radionuclides released into the surface mixed layer. As discussed in the conclusion (section 4), a future avenue of investigation would be three-dimensional trajectories (as the water parcels may subduct and move in 3D).

As there are many other environmentally important natural and anthropogenic biogeophysical tracers in Cape Cod Bay, such as red tide (McGillicuddy et al. 2014), turtle shock (Liu et al. 2019), or microplastics (Kosovsky 2022; Lermusiaux et al. 2019)

Corresponding author: Margaret Gregory, magregor@mit.edu

DOI: 10.1175/JPO-D-24-0023.1

that can be addressed with improved understanding of Cape Cod Bay circulation, a second goal of this study is to further explore near-surface currents and transport processes in the bay. One useful circulation characteristic is residence time, i.e., time spent by a water parcel inside a domain of interest before exiting. Previously, Geyer et al. (1992) reported that the surface waters of the larger Massachusetts Bay system have residence times of 20–45 days. However, with minimal observational data, Geyer et al. (1992) obtained a limited picture of residence time within Cape Cod Bay. During the study, from April 1990 to June 1991, eight drifters traveled into Cape Cod Bay, three of which were grounded within the bay. The other five drifters spent 4, 5, 14, 43, and ~30 days in the bay before exiting. In this research, we work toward a more detailed, spatially, and temporally varying picture of Cape Cod Bay transport characterization, mapping out residence times, times to reach the coast, and probabilities of exiting the bay throughout the entire domain in different seasons and years.

Previously, Geyer et al. (1992), using observations collected between November 1989 and June 1991, and Lermusiaux (2001) and Robinson and Lermusiaux (2001), using the Harvard Ocean Prediction System and data from the Massachusetts Bay Sea Trial 98 (MBST-98) (Beşiktepe et al. 2003), studied the mean circulation pattern of Massachusetts Bay including Cape Cod Bay. Additional observational and numerical studies looking at individual events and processes within the bay on daily to yearly time scales include Signell and List (1997), Robinson et al. (1999), Werme and Hunt (2005), Warner et al. (2008), and Jiang et al. (2007). In addition to a predominant cyclonic circulation within Cape Cod Bay that generally drives the surface flow, the researchers observe a persistent current flowing southward from the northwest region of Massachusetts Bay. As depicted in Lermusiaux (2001), Robinson and Lermusiaux (2001), and Beşiktepe et al. (2003), this current separates into two branches north of Cape Cod Bay around 42.1°N, with an inshore southward current (a) traveling into the bay along the western coast and an offshore southward current (b) diverting eastward, passing by Race Point, and flowing southward along the eastern shore of the Outer Cape. More recently, Rypina et al. (2022) revisited the geometry of the mean currents and found the mean current patterns to be generally consistent with the previous findings but with a third branch (c) peeling off the inshore southward current (a) flowing into the bay, before curving toward and around Race Point and merging with the offshore branch (b) going southward along the Outer Cape (Fig. 1).

Variations in the size, position, and even direction of the predominant cyclonic circulation due to winds and tides have been previously reported by Geyer et al. (1992), Beşiktepe et al. (2003), Robinson et al. (1999), Werme and Hunt (2005), Signell and List (1997), Warner et al. (2008), and Lermusiaux (2001). Robinson et al. (1999) and Lermusiaux (2001) both noted the short time scale upon which these changes can occur, with the circulation appearing cyclonic, anticyclonic, or absent all within less than a week. Given this variability in surface currents, velocity data with fine temporal resolution over multiple years (such as the 3-yr-long 6-hourly output from the realistic model GoMOFS used here) are required to better understand transport within Cape Cod Bay as well as the fate of a wastewater plume and/or other contaminants. Our analysis suggests that despite the short (order of days) time scale of the flow variability, the existence of a statistically robust picture of seasonally distinct transport pathways in Cape Cod Bay can be established.

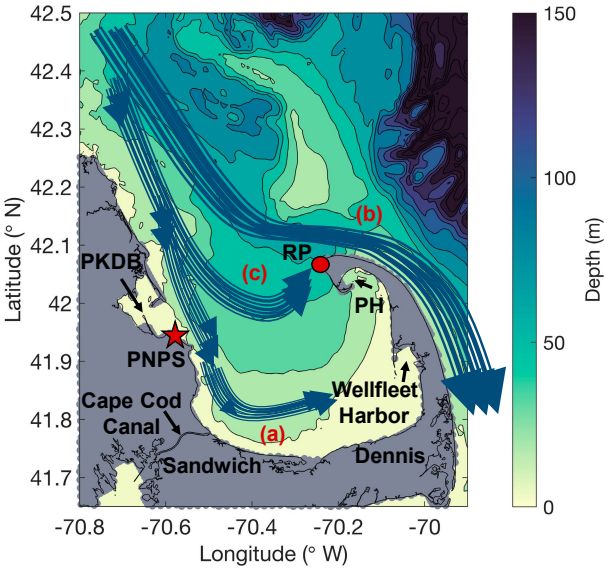

FIG. 1. Schematic of currents within and around Cape Cod Bay adapted from Rypina et al. (2022), with permission. Labeled geographical locations are mentioned in the text, with PKDB: Plymouth, Kingston, and Duxbury Bays; PH: Provincetown Harbor. A red star denotes PNPS, and a red circle marks Race Point (RP). The labels (a)–(c) show the three main current branches described in the text. Background is the depth of the bay in meters.

Data and methods are described in section 2. Results are presented in section 3, focusing first on the application to a PNPS wastewater release (sections 3a–d) and then on the overall transport structure in the bay (section 3e). Conclusions are provided in section 4.

2. Data and methods

a. *Model output and drifter data*

The area of interest for this study is Cape Cod Bay and its close surroundings, more specifically the region between 70.8°–69.9°W and 41.65°–42.5°N (Fig. 1). With a maximum zonal width across the bay of around 40 km and a maximum water depth within the bay of about 50 m, data with high spatial resolution are necessary to resolve the local dynamics. Our analysis utilizes surface velocity fields output from GoMOFS, a ROMS-based regional model with a domain reaching from the Nantucket Shoals to the Scotian Shelf, i.e., extending well outside of our area of interest. The four corners of the model domain are as follows: (38.5431°N, 69.8548°W), (41.7415°N, 61.2536°W), (46.1781°N, 63.9011°W), and (42.7894°N, 73.0352°W). The GoMOFS model has a spatial resolution of 700 m in the horizontal and 30 bathymetry-

following vertical layers, which are evenly spaced in shallow water (defined as being much less than 50 m) and stretched in deeper water with more layers near the surface than at depth (Shchepetkin and McWilliams 2005). The top model layer represents the surface flow and allows for fluctuations in sea surface height. The vertical extent (width) of the top layer varies from 0.2 m near the coastline to 1.5 m away from the coast. In addition to relatively high spatial resolution, GoMOFS output has a temporal resolution of 6 h and covers the time interval from 2018 to the present. Here, we focus on 2019–21.

The oceanic forcing and boundary condition information used by GoMOFS is generated by the Coastal Ocean Modeling Framework for NOAA's High Performance Computer (COMF-HPC) (Zhang and Yang 2014). The model domain extends well outside of our area of interest, minimizing the boundary effects, such as the velocity forcing [obtained from Real-Time Ocean Forecast System (RTOFS)] used at the open lateral boundary. The model's use of realistic tidal and atmospheric forcings works to represent seasonal-to-interannual variability. GoMOFS uses tidal forcings obtained from the Advanced Circulation (ADCIRC) EC2001 database which has a 1-h temporal resolution and resolves nine tidal constituents with a 1–4-km horizontal resolution along land boundaries (Mukai et al. 2002). GoMOFS' atmospheric forcing is obtained from the North American Mesoscale Forecast System (NAM) which supplies sea surface wind velocity components, air pressure, air temperature, air humidity, and longwave and shortwave radiation (Zhang and Yang 2014). This atmospheric forcing has a 3-h temporal resolution and a 12-km spatial resolution. See Yang et al. (2019) and Peng et al. (2018) for more information on GoMOFS' implementation.

Drifter trajectories from the NOAA fisheries "Drifter Tracks from the NE US Shelf and Beyond" Environmental Research Division's Data Access Program (ERDDAP) server allow for a comparison between the model and observations to validate our use of the model for this analysis. Between the start of 2019 and the end of 2021, the time period of this study, 20 drifters pass through the domain of interest. Most drifters in this dataset are of the Coastal Ocean Dynamic Experiment (CODE) type (Davis 1985a,b), with a position transmission rate of 1 h. The drifters' drogues are about 1 m deep and sit just underneath the ocean surface, effectively sampling the flow within the top 1 m of the water column. This depth is less than the depth of the second model layer throughout most of the domain of interest. For this reason, in our analysis, we assume that the top model layer reasonably approximates the flow at the depth of the drifters' drogues and use the first model layer velocity to advect simulated drifters.

b. Model validation

For Lagrangian model validation, we released simulated drifters at the location and time of the real drifters and advected them for the duration of the real drifter's lifetime using GoMOFS surface velocities. To test the sensitivity of simulated trajectories to the exact location and timing of the release, ensembles of nine simulated trajectories were also initialized on a regular 3×3 grid within 0.01° around each release location at the time of the real release, as well as 6 h before and after. From the simulated trajectories, we calculated the probability of a particle passing through a given $0.025° \times 0.025°$ bin in our domain and compared the values to the corresponding real drifter probabilities. For an even comparison, we only consider the simulated particles released at the exact time and location as the real drifters in this calculation, not the entire ensemble.

Simulated trajectories in all our calculations were estimated using the variable-step fourth-order Runge–Kutta integration scheme (ode45 in MATLAB), with absolute and relative tolerance values set to 10^{-9} (further decrease in tolerance did not lead to any changes in the calculated trajectories) and with bilinear interpolation in time and space between model grid points. The same integration and interpolation schemes were used in related prior work (Rypina et al. 2011, 2014, 2021, 2022). See appendix A for details on the accuracy of the variable time-step method used in this study as compared to the corresponding fixed time-step method.

Additionally, we validate the model's velocity fields by computing time-mean surface currents and eddy kinetic energy (EKE) maps and comparing them to previously published drifter-based maps [Figs. 1c,d in Rypina et al. (2022)]. Based on the same drifter dataset used in our model validation, Rypina et al. (2022) estimated EKE in the domain, showing that the current speed associated with the eddy component peaks north of Race Point and tends to exceed the mean velocity by 2 (or more) times in most of the domain.

For a comparison to Rypina et al. (2022), we released 417 particles (the same number of drifters used in their analysis) at random times and random locations within our domain. We chose randomized releases because only having 3 years of overlapping data between the model and drifter database prohibits the release of simulated particles at the same location and time as each real drifter. Trajectories for each simulated particle were estimated for 7 days, and the velocities of the particles were recorded every 6 h. To calculate the time-mean surface currents and EKE maps, we group the velocities by position in $0.025° \times 0.025°$ bins. The eddy field was defined as the deviation from the mean $\mathbf{U}_e = \mathbf{u} - \overline{\mathbf{U}}$ with $\mathbf{u}$ denoting the individual particle velocities, $\overline{\mathbf{U}}$ denoting the mean particle velocity for each bin, and $\mathrm{EKE}p = |\mathbf{U}_e|^2$. Here, the subscript p designates EKE calculated from simulated particle velocities.

For an Eulerian model validation, we also computed model-based time-mean (i.e., 3 year average over 2019–21) surface currents and EKE maps directly from the model velocity output. In this case, the eddy field was defined as the deviation from the mean $\mathbf{U}_e = \mathbf{u} - \overline{\mathbf{U}}$ with $\mathbf{u}$ denoting the full velocities, $\overline{\mathbf{U}}$ denoting the yearly mean velocity, and $\mathrm{EKE} = |\mathbf{U}_e|^2$. For ease of comparison between the mean velocity and EKE fields, we plotted the mean of $\mathrm{EKE}^{1/2}$, so that both variables had units of meters per second ($\mathrm{m\,s^{-1}}$).

c. Probability and travel time maps in simulations with PNPS wastewater release

Tracking large ensembles of simulated trajectories allows the identification of possible PNPS wastewater spreading

pathways. We released 100 trajectories every 6 h from 2019 to 2021 on a regular 10 × 10 grid in a 0.1° × 0.1° box around PNPS, which we specified as being centered at 41.94°N, 70.58°W. Out of the 100 particle release positions, only 56 were located in the ocean. Releases every 6 h resulted in a total of 245 280 individual trajectories for our analysis. Each trajectory was integrated for 3 weeks to allow sufficient time for particles to exit the bay or come into contact with land. In our calculations, particles can have a calculated position that is on land because the model does not resolve small-scale currents along the shore. When this occurs, we choose to leave the particle on land, effectively stopping it, instead of manually placing it back into moving water. This choice of the integration time, which is at the lower limit than that suggested by Geyer et al. (1992), was motivated by the results of Rypina et al. (2022) who determined that drifters exited or reached the easternmost parts of the bay (located furthest from PNPS) in less than 2 weeks.

Sectioning the domain into bins and dividing the number of trajectories that pass through each bin by the total number of trajectories resulted in the probability of a simulated particle originating off the coast of PNPS traveling to a specific region within the domain. Connected bins with the highest probabilities illustrate the most probable spreading pathways. For the results presented here, we divided the domain into 0.01° × 0.01° bins (i.e., 825 m × 825 m), slightly larger than the model's horizontal resolution. Changing the bin sizes alters the resolution of the probability maps and the magnitudes of the probabilities in each bin but preserves the general patterns of the probable spreading pathways.

We also present travel time maps, which are associated with each probability map, that quantify the average time for a particle to travel from its initial position to a given bin within the domain. In our analysis, travel times were estimated as the ensemble average over all trajectories passing through a bin.

d. *Residence times, probabilities to leave the bay, and probabilities to get onshore in simulations covering the entire bay*

In the second part of the paper, we are interested in quantifying transport properties over the entire bay, rather than specifically for a PNPS wastewater release. For these simulations, we released 1500 trajectories every 6 h from 2019 to 2021 in a 0.70° × 0.38° box which encompasses the bay (from 70° to 70.7°W and from 41.72° to 42.1°N) on a regular grid with a zonal grid size of 0.0140° of longitude and a meridional grid size of 0.0127° of latitude. Each trajectory was integrated for 60 days. This choice of integration time was motivated by the results from Geyer et al. (1992), where the longest residence times for the bay were estimated to be 45 days. Examination of the final positions of our simulated trajectories after 60 days also suggests that this integration time is indeed sufficient for the majority of trajectories to either leave the bay or reach the shore (see appendix B for more detail).

Specific quantities of interest are residence times within the bay, probabilities to leave the bay, and probabilities to get onshore. Residence times correspond to the time at which each trajectory exits and remains outside of the bay. If a simulated particle exits, but then reenters, the time of exit was not recorded, and if a particle exits, reenters, and then reexits the bay, the last time of exit was recorded as the residence time. The average residence time in a given bin was estimated as an ensemble average over all trajectories with valid residence times released from that bin. If a particle does not exit in 60 days, it does not have a valid residence time and is not included in this average. Probability of leaving the bay was straightforwardly estimated as the number of trajectories that exit divided by the number of trajectories released. Probability of reaching the coast was similarly estimated as the number of trajectories that end up on land divided by the number of trajectories released.

Here, we defined "out of the bay" as a region north of 42.15°N to the west of Race Point and north of the Outer Cape coast to the east of Race Point. Note that 42.15°N is located slightly north of Race Point, so that trajectories that meander around the latitude of Race Point were still counted as being in the bay. While our choice of the exact latitude of the northern boundary of the bay is somewhat arbitrary, after 60 days, there are very few trajectories with final positions to the northwest of Race Point (Fig. B1 in appendix B). Instead, most trajectories that are destined to leave the bay tend to rapidly flow eastward north of Race Point and then southward along the Outer Cape. Therefore, our results are nearly insensitive to the exact latitude of the northern boundary of the domain to the west of Race Point. See appendix C for further discussion of our domain definition and the boundary at 42.15°N based on sensitivity experiments.

e. *Ekman currents*

In investigating the response of the spreading to wind forcing, we chose to calculate Ekman currents from wind data because the model does not provide the Ekman component of the velocities as an output but does provide wind velocity data on the same horizontal and temporal grid as the surface velocities. Using the model's wind forcing, we separated out the wind-driven component of the model's full velocity solutions by calculating the induced Ekman currents within Cape Cod Bay using the formulation from Pond and Pickard (1983) in which

$$u_{\mathrm{ek}} = V_0 \cos\left(\frac{\pi}{4} + \frac{\pi}{d_{\mathrm{ek}}} z\right) \exp[(\pi/d_{\mathrm{ek}})z], \tag{1}$$

and

$$v_{\mathrm{ek}} = V_0 \sin\left(\frac{\pi}{4} + \frac{\pi}{d_{\mathrm{ek}}} z\right) \exp[(\pi/d_{\mathrm{ek}})z]. \tag{2}$$

Here, the Ekman depth is given by $d_{\mathrm{ek}} = \pi\sqrt{2A_z/|f|}$ with A_z as a constant eddy viscosity and f as the Coriolis parameter. Additionally, $V_0 = \sqrt{2}\pi\tau/(d_{\mathrm{ek}}\rho|f|)$ is the Ekman surface current and $\tau_{x,y} = \rho_{\mathrm{air}} c_d \mathbf{U}\mathbf{u}_R$ is the magnitude of the wind stress with $\mathbf{U} = \sqrt{u_R^2 + v_R^2}$ and $\mathbf{u}_R = (u_R, v_R)$ as the model winds rotated such that they are directed along the y axis or positive meridional direction.

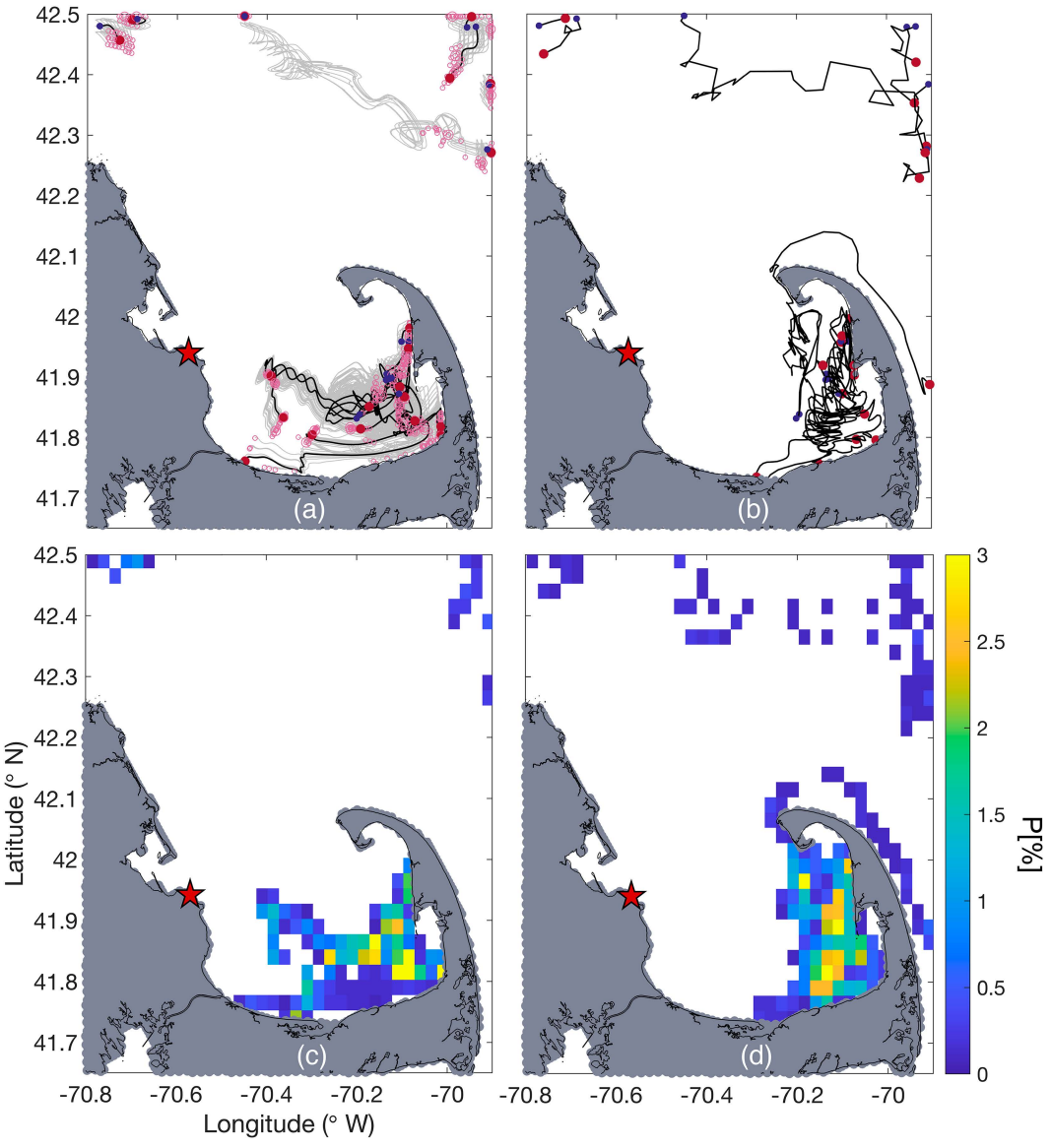

FIG. 2. Comparison between (a) simulated and (b) real drifter trajectories. In (a), black curves denote simulated trajectories of particles released at the exact time and position as the actual drifters. Filled blue circles mark the starting location, and red circles mark the final position. The gray curves in (a) show ensembles of simulated trajectories released around (±0.01° in zonal and meridional directions) the actual drifter release location at the time of the real release, as well as 6 h before and after and have final positions denoted by open pink circles. The real drifter tracks in (b) are represented by the black curves. Filled blue circles mark the starting location, and red circles mark the final position. Probability of (c) a simulated particle or (d) a real drifters passing through a 0.025° × 0.025° bin in the domain. A red star marks the position of the PNPS.

Using the formulation from Pond and Pickard (1983), both the magnitude and direction of the Ekman currents can be calculated at each depth z. Given the form of Eqs. (1) and (2), the magnitude of the Ekman currents will decay exponentially with depth, while the direction spirals to the right starting at a 45° angle right of the winds at the surface. In our analysis, the Ekman currents are computed at 1 m below the surface (because of our focus on near-surface transport).

3. Results

a. *Model validation*

To validate the model, we compared the real drifter trajectories to simulated trajectories (Fig. 2). Overall, we observe qualitatively similar trajectories and a similar distribution of final positions. Specifically, Wellfleet and Provincetown Harbors are devoid of trajectories, with the majority of both real and simulated drifters remaining in the southeastern elbow of

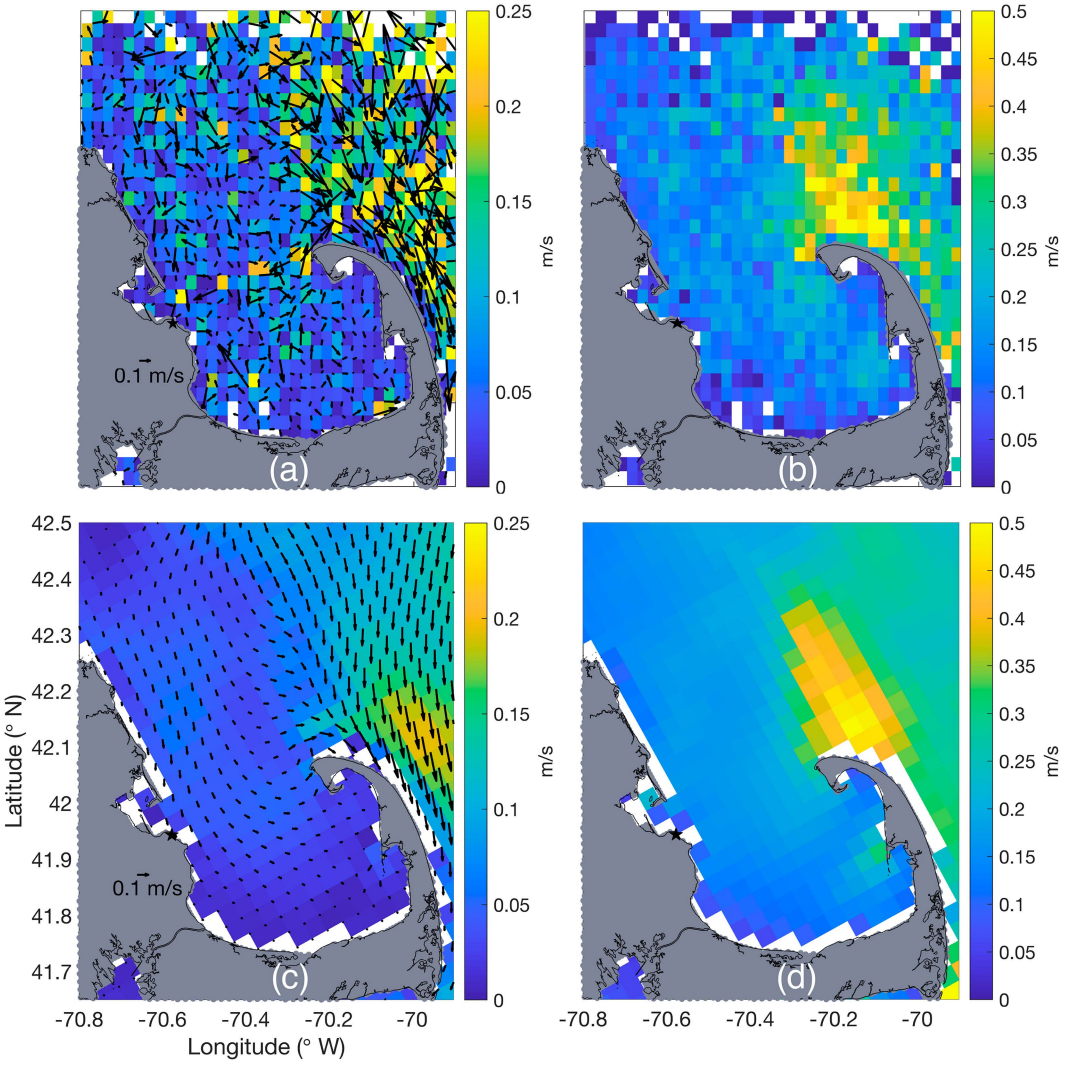

FIG. 3. (a) Mean surface velocity field from simulated particles integrated on model surface velocity fields. (b) Square root of mean simulated particle EKE $\sqrt{\text{mean}(\text{EKE}_p)}$. (c) Mean model surface velocity field. (d) Square root of mean model EKE $\sqrt{\text{mean}(\text{EKE})}$. (c),(d) Utilize four times daily GoMOFS velocity fields from 2019 to 2021.

the bay, from Dennis to Kingston at 42°N. Note that the movement of the drifters, both real and simulated, is typically not well represented by the mean cyclonic circulation characteristic of the currents in the bay; this is due to the energetic transient currents, as indicated by the high EKE within the bay compared to the mean (see Figs. 3b,d). Additionally, calculating the probability of a particle/drifter passing through a given bin in the domain reveals higher probabilities between 70.2° and 70.15°W within the bay for both the simulated trajectories and real drifter tracks (Figs. 2c,d).

The real and simulated drifters disagree for one real drifter released on 31 October 2019 that escaped the bay via curving around Race Point as well as for two drifters at the northwesternmost locations. For the northwesternmost drifters, despite heading in the wrong direction, the simulated trajectories are equally short as the real trajectories, correctly suggesting weak current speeds in that area at the time. Also, some simulated trajectories extend slightly further west compared to real drifters.

The mean velocity field calculated from the 2019–2021 GoMOFS surface velocities (Fig. 3c) shows a weak (0–0.05 m s^{-1}) cyclonic gyre in the bay, with stronger eastward currents (about 0.15 m s^{-1}) in the channel just north of Race Point and strongest southward currents (0.20–0.25 m s^{-1}) along the Outer Cape, all in full agreement with our simulated trajectory-based mean velocity estimate (Fig. 3a) and the real drifter-based mean velocity estimate of Rypina et al. (2022). Strong agreement is also seen between our EKE field calculated from the Eulerian GoMOFS output (Fig. 3d), the simulated trajectories (Fig. 3b), and the real drifter data [Fig. 1d in Rypina et al. (2022)]. All three model- and drifter-based EKE maps show maximum mean EKE values reaching 0.5 m s^{-1} to the north and northeast of Race Point, with lower—O(0.15–0.25) m s^{-1} values—in

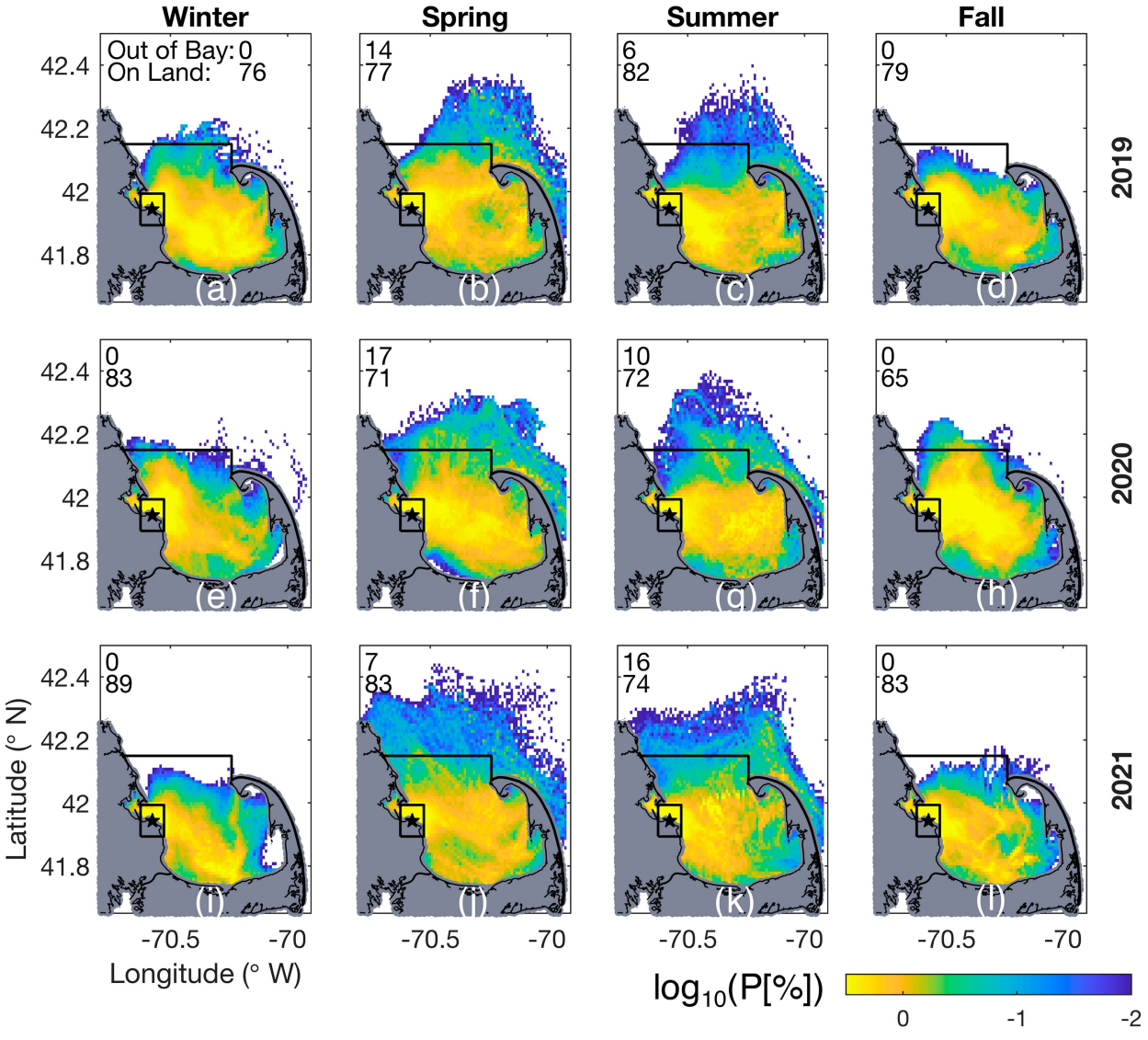

FIG. 4. Probability map (log scale for visibility) showing the probability of a simulated particle released off PNPS passing through a given bin in the domain. Prominent spreading pathways are represented by yellow. Dark blue denotes areas reached by only a small number of particles. White indicates zero probability. The 0.1° × 0.1° release box is outlined in black with a black star denoting PNPS location. Uppermost value in the left-hand corner is the probability of a particle exiting the bay (defined by a final position north of the black line), and the bottom value is the probability of a particle ending up on land in percentages.

the bay. In both drifter- and model-based maps, there is an indication of an increase in mean velocity and EKE in the bay offshore of Wellfleet.

The real drifter-based maps are generally noisier than their Eulerian model counterparts (likely due to the limited number of drifters) and present more widespread peaks in both mean velocity and EKE north and northeast of Race Point, which could be a consequence of the different time averaging windows—over 20 years for drifters versus 3 years for GoMOFS. The simulated trajectory-based maps are also noisier than their Eulerian model counterparts since we limit the number of trajectories to match the data availability of the real drifters. Repeating the calculations of time-mean velocity and EKE using a greater number of randomized releases reduces the noise and increases agreement between the Lagrangian and Eulerian model–based maps.

b. *Probable spreading pathways of a PNPS wastewater plume*

Probability maps (Fig. 4) suggest strong seasonality in the spreading pathways of a PNPS wastewater plume. Simulated particles released during winter (January–March) and fall (October–December) almost entirely remain in the bay, whereas some particles released in spring (April–June) and summer (July–September) do leave the bay. That is, probability values outside of the bay are virtually zero in winter

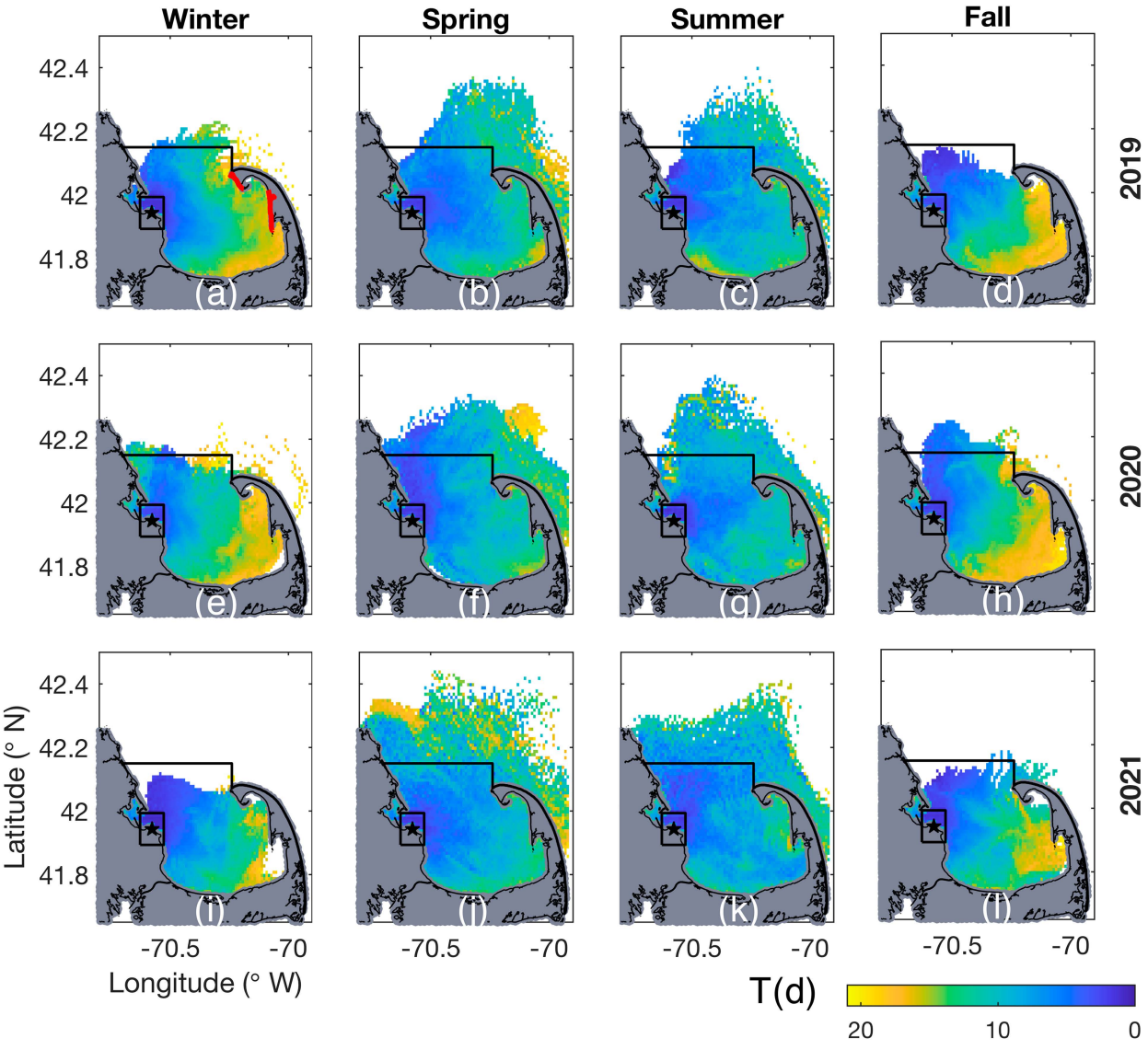

FIG. 5. Travel time map (days) showing the average time that it takes for a simulated particle released off PNPS to reach a given bin. White indicates areas not reached by the particles. Black release box, black star, and out-of-the-bay boundary as in Fig. 4. Red coastlines in (a) denote the regions used to estimate the average travel times across the bay.

and fall, i.e., white with minimal blue, whereas nonzero probabilities, i.e., blue/green/yellow, are observed north of the bay, north of Race Point, and along the Outer Cape in spring and summer for all 3 years.

In all seasons, the most likely spreading pathways, denoted by the brightest yellow, generally tend to be confined to the bay. A yellow blob of high probability is always present near the release location, and the yellow stripes can often be traced from PNPS toward Dennis along the southern shore of the bay, toward Wellfleet to the east, or to Provincetown. Probabilities are also high in Plymouth, Kington, and Duxbury Bays (although the limited spatial and temporal model resolution is inadequate to fully resolve transport in these areas). Other notable features of the transport that are present during all seasons include low probabilities inside of Provincetown and Wellfleet Harbors. Most strikingly, Provincetown Harbor is completely blocked from the potential wastewater during winter and fall 2019 and 2021 and Wellfleet Harbor is partially or fully blocked in winter 2020 and fall/winter 2021. Additionally, the area offshore of Sandwich (near Cape Cod Canal which is closed in our model) is usually characterized by decreased probabilities.

Even with an increase in the probability of simulated particles exiting the bay during spring and summer compared to fall and winter, the probability of leaving the bay remains small. The average probability of exiting the bay in spring and summer is only 12%. The probability maps suggest that the particles released off PNPS are more likely to wash up on land inside the bay than to exit the bay. There is a minimal increase in probability of reaching land in winter and fall compared to spring and summer (79% vs 77%).

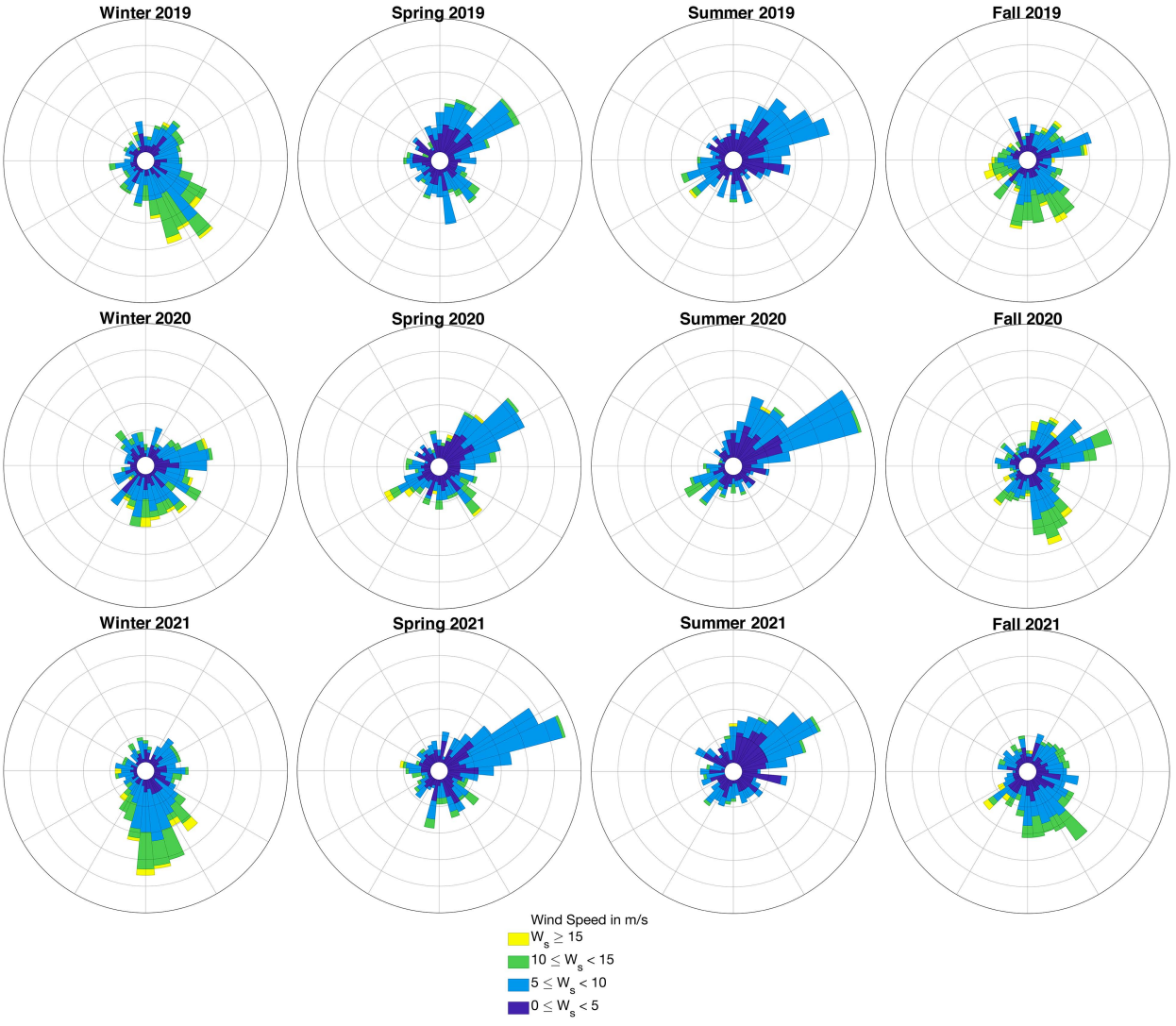

FIG. 6. Wind roses, which classify the wind by magnitude and direction (in which the wind is heading, not from which it is coming from), at (41.94°N, 70.23°W) for different seasons and years. Wind roses plotted using code developed by Pereira (2020).

Similar to the probability maps, persistent seasonality once again emerges in the travel time maps (Fig. 5). Specifically, particles released during winter and fall (yellows) experience slower travel times crossing the bay than particles released during spring and summer (blues and greens). On average, particles cross the bay and reach the tip of the peninsula at the entrance of Wellfleet Harbor in approximately 17 days during winter/fall and in around 11 days during spring/summer. Similarly, winter and fall releases correspond to longer average travel times of around 13 days to reach Race Point, versus 8 days for spring and summer. In cases where a direct pathway to Race Point is observed, spring 2019 and summer 2020, for example, average travel times to the bins along the coast can range from 5 to 7 days, the upper range of the 3–6-day estimate suggested by the full database of real drifters (Rypina et al. 2022). Average travel times for crossing the bay are computed by averaging over the bins offshore of the eastern coastlines noted in red in Fig. 5a. The region used is two bins wide in the offshore direction.

Some degree of interannual variability is observed in both the probability and travel time maps over all seasons, but is relatively weak compared to the robust and persistent seasonal trends.

c. *Effects of wind*

Many researchers, such as Geyer et al. (1992), Lermusiaux (2001), and Warner et al. (2008), identify Cape Cod Bay as a region strongly influenced by wind. Thus, it is natural to hypothesize that the seasonality in transport observed in Figs. 4 and 5 directly relates to seasonal variations in wind-driven surface currents. With this in mind, we turn to the wind forcing and examine the resulting Ekman currents. The winds over Cape Cod Bay exhibit strong temporal variability but are nearly spatially uniform and can be well described by the magnitude and

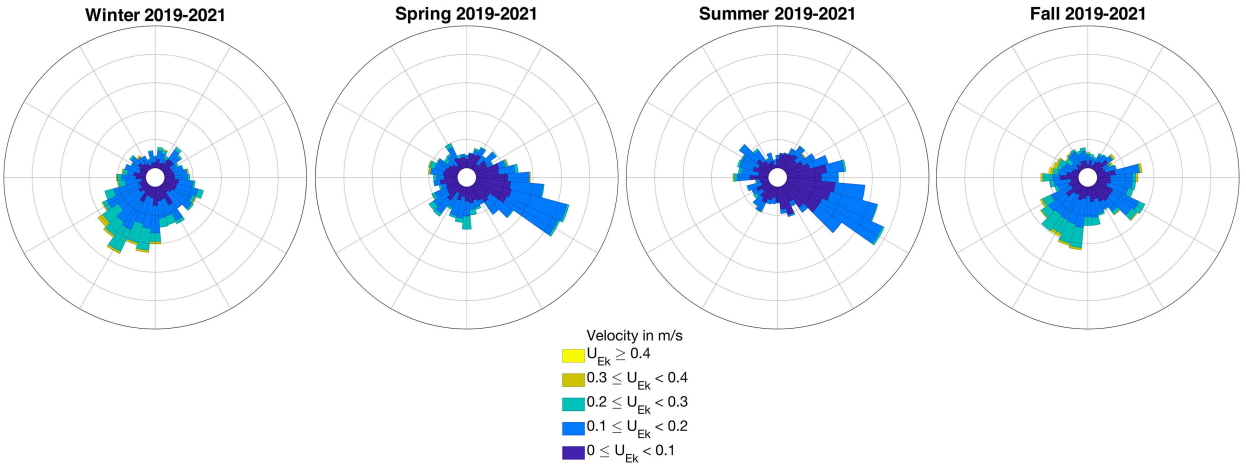

FIG. 7. Ekman currents at 1 m below the surface calculated from the wind data plotted in Fig. 6 using Eqs. (1) and (2) and grouped by season.

direction recorded at the center of the bay (41.94°N, 70.32°W). Examining seasonal wind rose diagrams for 2019–21 (Fig. 6), we see that, in agreement with Geyer et al. (1992), seasonality emerges, with stronger southeastern (i.e., coming from northwest) winds often reaching or exceeding 15 m s^{-1} during winter and fall and weaker northeastern winds below 10 m s^{-1} during spring and summer.

The seasonality in the winds is reflected in the near-surface Ekman currents (Fig. 7), indicating stronger southwestward Ekman currents reaching 20–40 cm s^{-1} in winter and fall versus weaker, <20 cm s^{-1}, southeastward Ekman currents in spring and summer. We also looked at the Ekman current roses in the four corners of the bay, specifically at (41.821°N, 70.430°W), (41.942°N, 70.135°W), (42.017°N, 70.479°W), and (41.827°N, 70.242°W), finding them to be qualitatively and quantitatively the same. A connection could be implied between strong southwestward Ekman currents pushing water into the bay and suppressing out-of-the-bay transport during the winter and fall seasons.

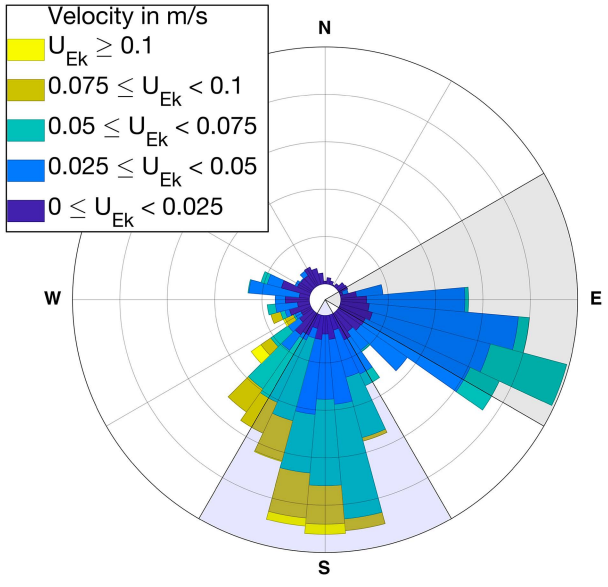

FIG. 8. Ekman currents from 2019 to 2021 after performing a 3-week running average. The purple/gray sectors correspond to the southward/eastward directions used to classify the trajectories.

To solidify this idea, we classified our simulated trajectories into six categories according to the associated direction (Fig. 8) and magnitude (Table 1) of the predominant Ekman currents, determined by performing a 3-week running average over the duration of each trajectory. Probability maps for each category reveal changes in spreading pathways due to wind conditions (Fig. 9). For the strong and medium southward Ekman currents (Figs. 9a,b), out-of-the-bay transport is strongly suppressed, with the probability of leaving the bay an order of magnitude smaller (0%–0.4%) than that for the remaining categories, i.e., for the weak southward and medium/weak eastward Ekman currents (when the probability of leaving the bay is 6%–15%).

The corresponding travel time maps for the six categories (Fig. 10) suggest faster eastward advection across the bay to Wellfleet and the southeastern corner of the bay for eastward Ekman currents (blues and greens) compared to southward Ekman currents (yellows).

Key characteristics of transport (travel times, spreading direction, and probability of leaving the bay) during the different seasons and wind conditions (Table 2) are similar for winter/fall seasons and strong/medium southward Ekman currents, as well as for the spring/summer and eastward Ekman currents. This is

TABLE 1. Threshold values (i.e., 25% and 75% percentiles by magnitude for 3-week averaged Ekman currents at 1 m) used to classify Ekman currents into strong (the top 25%), medium (25%–75%), and weak (bottom 25%) categories.

Year	First quartile (m s^{-1})	Third quartile (m s^{-1})
2019	0.0223	0.0668
2020	0.0219	0.0657
2021	0.0273	0.0820

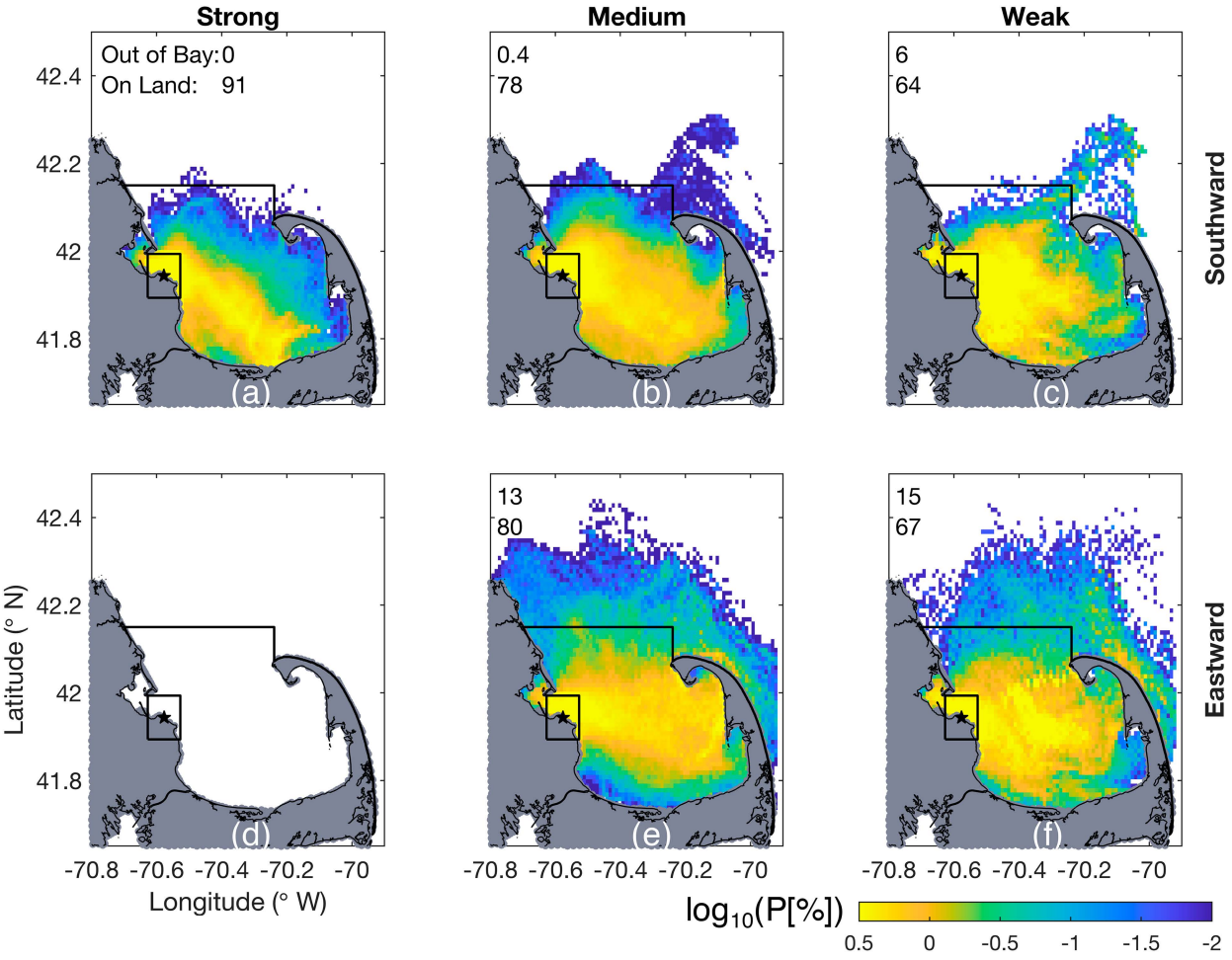

FIG. 9. (a)–(f) Probability maps (log scale for visibility) for the six categories of trajectories based on the associated Ekman currents. Numbers in the upper-left corner give the probability of particles exiting the bay, defined by a final position north of the black line, and the probability of particles ending on land in percentages. There is no color in (d) since zero particles experience strong, eastward Ekman currents on average over the integration period.

not surprising given that the winds during winter/fall are mainly higher magnitude and to the southeast (corresponding to Figs. 9a, 9b, 10a, and 10b), whereas winds during spring/summer are more likely to be weaker and to the northeast (corresponding to Figs. 9e, 9f, 10e, and 10f).

d. Sensitivity to release location

The final question we investigated in connection with a potential PNPS wastewater release was sensitivity to the location of release. We were interested in seeing whether the probability of exiting the bay would change significantly if the wastewater were to be released further offshore (although in real life, extending the wastewater pipe over long distances would be difficult). As mentioned in the introduction, in addition to investigating the fate of a potential wastewater plume, we were also interested in a more general question of understanding transport processes and their drivers over the entire bay. The calculation in this section is probably more relevant for the latter goal than the former.

Specifically, we trace particles that exit the bay back to their initial positions and record the number of particles that correspond to each release location. This technique allows us to determine which initial positions result in the most particles exiting the bay. The results are summarized in Fig. 11, which shows the probability of a trajectory leaving the bay within 3 weeks of release starting at a particular location within the release box. A pronounced pattern is observed, with probabilities increasing toward the northeast corner of the release box suggesting that particles released further from shore are more likely to exit the bay than those released along the coast.

e. Residence time

We now turn our attention away from the specifics of a potential PNPS wastewater release and extend our methods to address the more general question of transport in Cape Cod Bay. In this section, we characterize key features of transport throughout the region by describing the behavior of particles

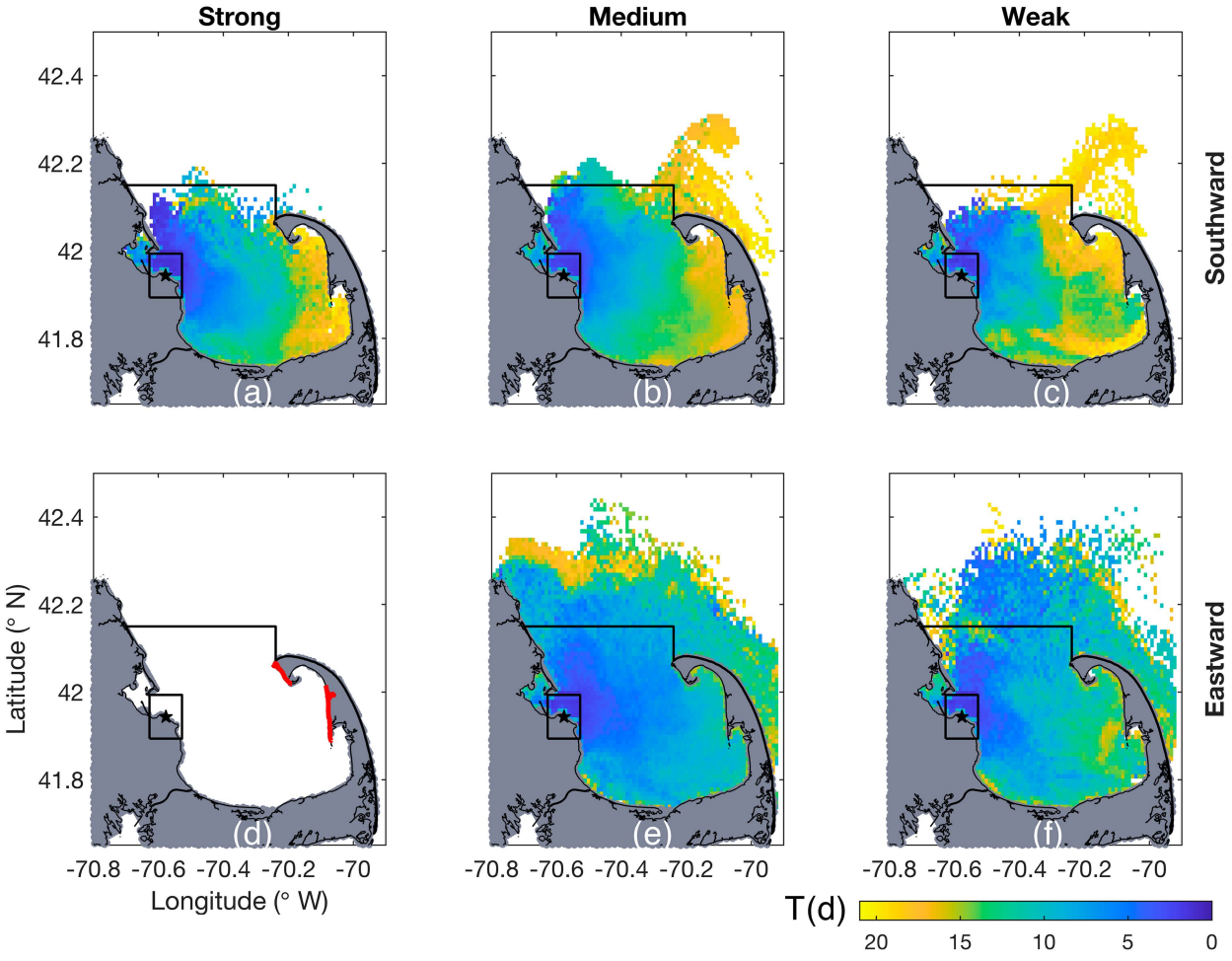

FIG. 10. (a)–(f) Travel time map (days) for the six categories of trajectories based on the associated Ekman currents. Red coastlines in (d) denote the regions for which average travel times are reported.

released throughout the entire bay. Residence times in the bay (Fig. 12) are strongly seasonal, with longer residence (purple colors or black circles) in winter/fall and shorter (lighter colors) in spring/summer. Not surprisingly, shortest residence times are seen over the northern part of the bay (north of the approximate latitude of PNPS) and specifically in the east near the tip of Cape Cod. The southeastern elbow of the bay, including Wellfleet Harbor and adjacent areas, is generally characterized by long residence times. Provincetown Harbor, or at least its southern part, also typically has long residence times. In the southwestern bay, residence times change dramatically with season, with longer residence times in winter/fall and shorter in spring/summer. It is the seasonality of the residence time in the southwestern bay that is likely the primary driver of the changes in the domain-averaged residence time of the bay. Note that because about 92% of particles are still in the bay after 60 days, the residence time for the particles that exit the bay in 60 days is different—much shorter—than the residence time for all particles in the bay.

Seasonal variations are also observed in the probability of particles released in the bay exiting in less than 60 days

TABLE 2. Summary of key transport features for different seasons and under different Ekman currents.

	Time to Wellfleet (days)	Time to Race Point (days)	Probable spreading pathways	Probability of exiting the bay (%)
Winter and fall	17	13	Dennis, Wellfleet, minimal northward spread	0.2
Spring and summer	11	8	Wellfleet, Race Point, northward spread	12
Strong and medium southward Ekman	17	13	Dennis, minimal northward spread	0.2
Eastward Ekman	15	9	Wellfleet, Race Point, northward spread	14

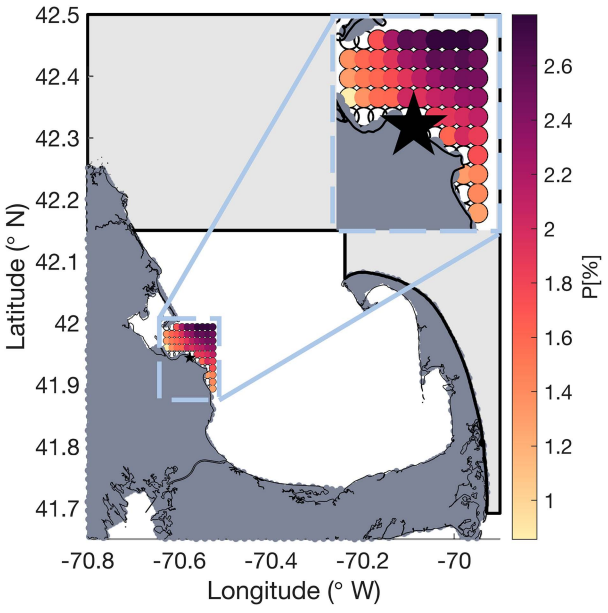

FIG. 11. Probability of initial position (represented by black circle outlines) for simulated particles that leave the bay within 3 weeks of release. As before, particles that exit the bay were defined as having their final positions within the light gray shaded region.

(Fig. 13). A nearly 10-fold increase in the domain-averaged probability is seen in spring/summer compared to fall/winter. An apparent correlation is observed between the spatial structure of the exit probability (Fig. 13) and the residence times (Fig. 12), with large probabilities confined to the areas with short residence times. The probability of exiting the bay is always highest (bright yellow) near Race Point and decreases rapidly to the south and less rapidly to the west. Probability of exiting from the southeastern corner of the bay, Wellfleet Harbor, and Provincetown Harbor is always small. Probabilities over the western part of the bay vary strongly with season (small in winter/fall and larger in spring/summer).

Generally, small exit probabilities over most of the bay, as well as widespread areas characterized by trajectories that do not leave the bay in 60 days, indicate that 2 months after the release a large number of simulated particles are still either circulating around the bay or have come onshore. We investigated this phenomenon further by calculating the percentage of particles that end up on land within Cape Cod Bay after 60 days (Fig. 14). Areas with low exit probabilities (Fig. 13) have high arrival onshore probabilities (Fig. 14). Again, strong seasonality arises, with higher chances of hitting land in winter/fall compared to spring/summer. Averaged over the full release domain and over 3 years, the probability of ending up on land is always high—87% in spring/summer and 94% in winter/fall. We note that the spatially averaged probability inside the red contours is not identically 100% as some particles from these initial positions are still traveling within the bay (without having come into contact with land) after 60 days.

The sum of the low probability of leaving the bay and high probability of getting on land is typically in the upper 90% range, implying that only a small percentage of simulated particles are still traveling within the bay after 60 days. Looking at the average distribution of particles after 60 days confirms that the majority of particles are either on land or out of the bay (Fig. B1).

Zooming in on the initial release box near PNPS (used in section 3b) suggests that the seasonality that we observed on a 3-week time scale still holds after 60 days; i.e., it is still the case that more simulated particles exit the bay when released in spring and summer. The minimal northward spread during winter and fall in Fig. 4 is reflected by longer residence times and a small percentage of particles exiting the bay in Figs. 12 and 13. Shorter residence times within the release box in Fig. 12h are representative of the northward spread seen in Fig. 4h. Similarly, shorter residence times and a larger probability of exiting the bay in 60 days seen within the release box during spring and summer in Figs. 12 and 13 reflect the increased northward spread and faster travel times observed in Figs. 4 and 5. See appendix D for further discussion of the seasonality, focusing on the effects of wind-driven circulation on the residence times.

4. Conclusions

Within the context of a possible PNPS wastewater release, we find that after 3 weeks since simulated discharge, particles released in spring and summer have a greater probability of exiting the bay than those released in winter and fall, when the out-of-the bay transport of a potential PNPS wastewater plume is nearly completely blocked. Even in spring and summer, the probability of leaving the bay remains low, with nearly all of the plume remaining in the bay for over 3 weeks. Most particles reach land over this time. Part of the plume that does leave the bay passes just north of Provincetown, hugs the coastline, and flows southward along the Outer Cape. Within the bay, the most probable spreading pathways extend from PNPS toward Wellfleet, Dennis, and Provincetown. Faster travel times to both Race Point and Wellfleet are seen for spring and summer releases compared to fall and winter. Knowing the probable final destinations and the time scale over which a wastewater plume is advected can help predict which areas would be affected and when.

The above characteristics of transport agree well with the long-time-mean drifter-based results of Rypina et al. (2022), who also observed likely spreading pathways extending from PNPS toward Dennis and Provincetown. The third, "northern," likely pathway in that study did lead out of the bay by first heading northward but then taking a sharp turn toward Race Point, passing just north of Provincetown, hugging the coast, and heading southward along the outer shelf, again consistent with the route we see in our model-based analysis for the water to leave the bay. The pronounced seasonal variability and the decrease in out-of-the-bay transport in fall and winter suggest that the drifters that took the northern pathway in Rypina et al. (2022) were likely released in spring and summer.

We also demonstrate that seasonality in spreading pathways is reflected and likely caused by seasonality of the winds and the resulting wind-driven Ekman currents in the upper

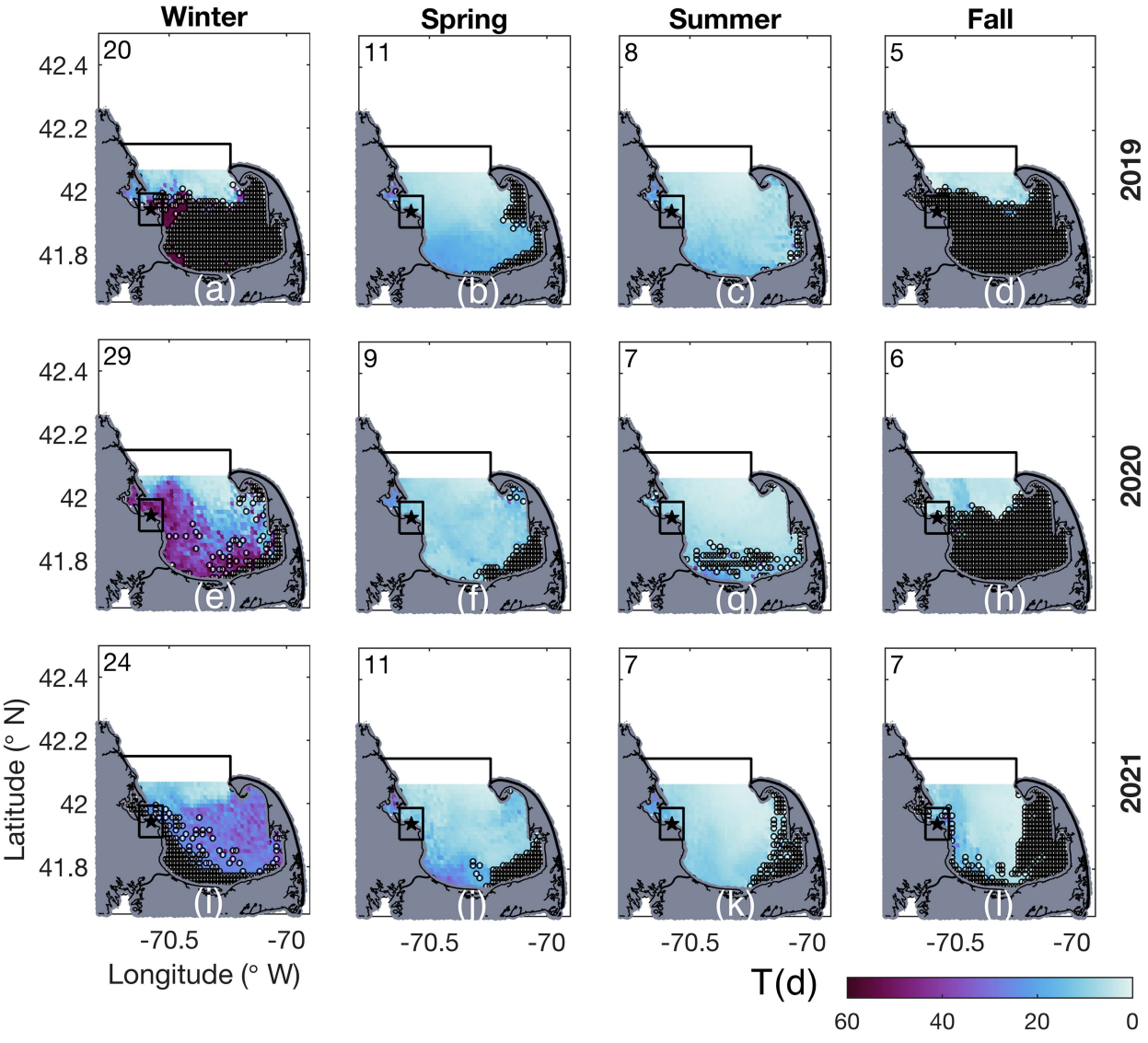

FIG. 12. Average residence time (days) for release locations located across the full bay. Black circles indicate locations from which no particles exited the bay after 60 days. Numbers in the upper-left corner indicate the domain-averaged residence times in days and exclude initial positions from which zero particles exited the bay in 60 days.

ocean. Strong southwestward Ekman currents are predominantly present during the winter and fall, which push and entrap water in the bay and suppress out-of-the-bay transport. On the other hand, during the spring and summer, Ekman currents are weaker and mostly southeastward and tend to advect particles toward Race Point, making it easier to leave the bay.

Looking at the bay at large, the domain-averaged probability of leaving the bay in 60 days is always low, 1%–4% in winter and fall and 6%–14% in spring and summer. The southeastern part of the bay including Wellfleet Harbor and surrounding areas has a nearly 0% of leaving, as does part of Provincetown Harbor. Not surprisingly, the probability of leaving is greater for simulated particles in the northern part of the bay. It is interesting that in winter and fall, the zonal boundary between waters to the south that do not leave the bay in 60 days and waters to the north that have nonzero chance of leaving is often located close to the latitude of PNPS, pointing to the strong sensitivity of the fate of a PNPS wastewater plume to its release location. Low overall probabilities to leave the bay, as well as long overall residence times within the bay (except in areas close to the northern opening of the bay), are explained by a high probability of particles reaching the shore (and getting stuck there). We note that the probability of exiting the bay during spring/fall 2021 is a little higher/lower than in 2019 and 2020. The winds for 2021 are not distinctly different from other years, and an interesting continuation of our analysis would be investigating whether the variability other than winds could be the cause of this anomaly. Even though the observed interannual variation is

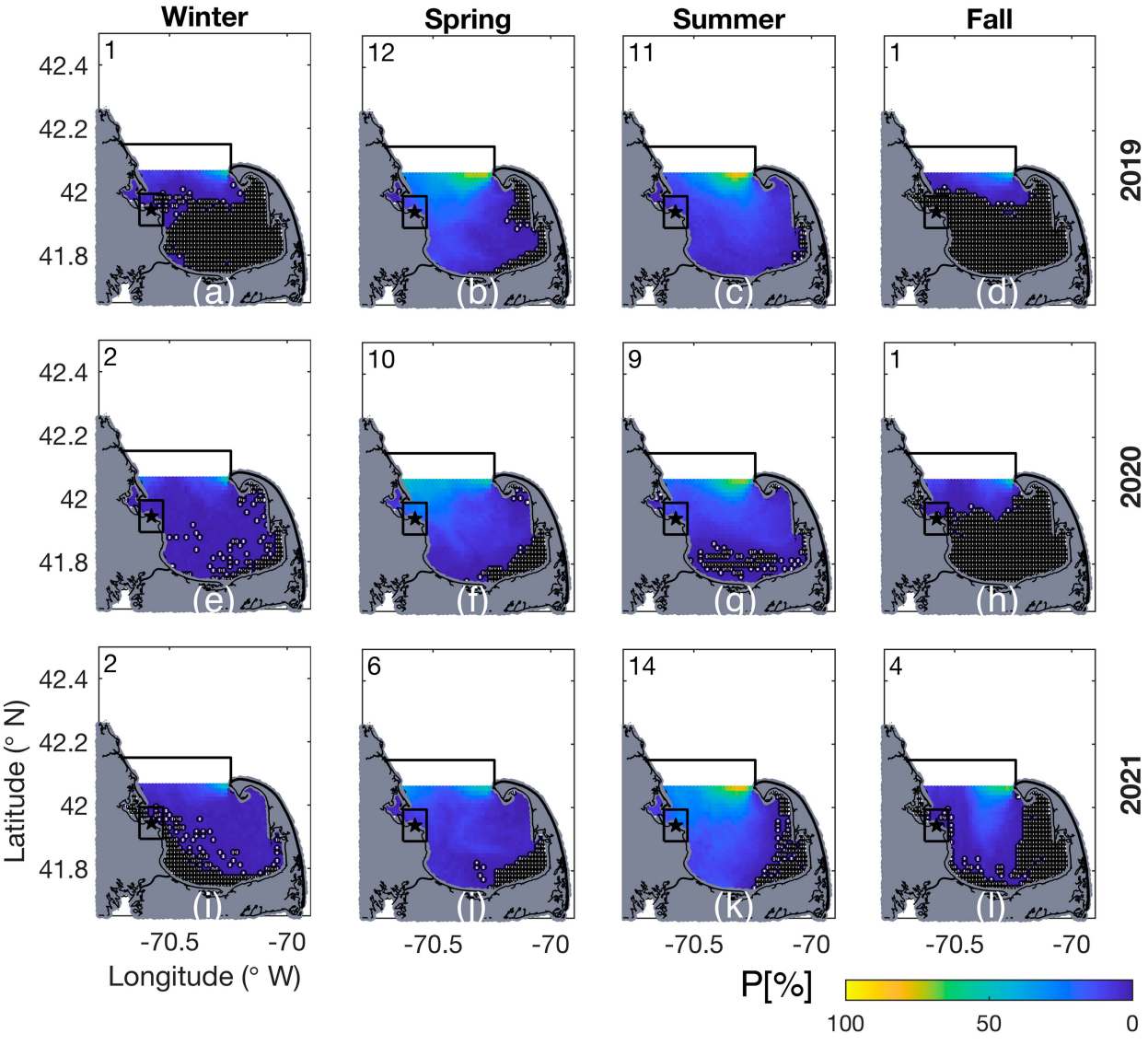

FIG. 13. Average probability of a particle exiting the bay for each release location. Black circles indicate regions from which no particles exited the bay after 60 days. Numbers report the domain-averaged percentage of particles that exit the bay within 60 days.

much smaller than seasonal changes for all 3 years analyzed, suggesting that other years would likely yield similar results, a useful continuation of this study could include analysis of additional years of data to see whether similar anomalies show up.

Our analyses focus exclusively on the physical advection of water by the near-surface oceanic currents and do not take into account chemical changes in the potential wastewater composition, natural radioactive decay, nonwater following effects for those radionuclides that do not fully dissolve in water, or absorption by sediments that will likely be important given the tendency of the particles in our model to come in contact with the coast. As the only current data GoMOFS provides as output are the full ocean currents, we calculated Ekman currents from the model's wind data. We used the method described by Pond and Pickard (1983) that assumes constant eddy viscosity to convert wind stress into Ekman currents. In the future, it would be interesting to use one of the more sophisticated methods described in Price et al. (1986), Price and Sundermeyer (1999), Brink (2023). We note that with a 700-m horizontal resolution, GoMOFS is unable to realistically resolve small-scale flow features along the geometrically complex shoreline of Cape Cod Bay. Also, GoMOFS does not allow for the opening through Cape Cod Canal which would allow transport of the possible wastewater into Buzzards Bay and might influence currents and transport in Cape Cod Bay. In addition, the 6-hourly temporal resolution of the GoMOFS output prevents the investigation of processes, including tides and sea–land breezes (Gille et al. 2005; Miller et al. 2003), that occur on time scales of about a day or

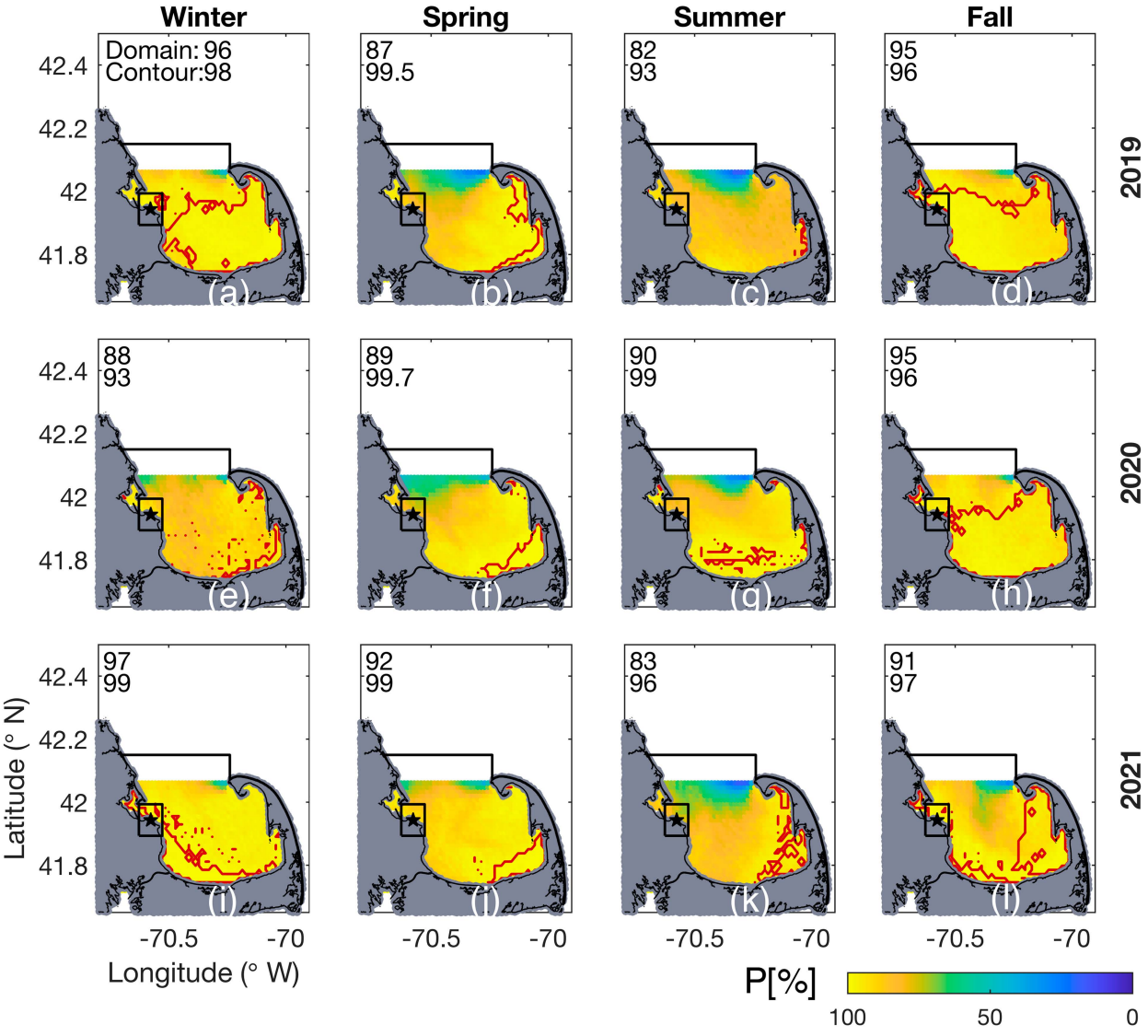

FIG. 14. Probability of a simulated particle having a final position on land after 60 days as a function of initial position. Red contours outline the regions from which zero particles exit the bay (i.e., regions covered with black circles in Figs. 12 and 13). Spatially averaged probability is calculated over the whole domain and over the area within the red contours for each season and displayed in the corner of each subplot.

less. Even though the model forcing fields (with 1 hourly tidal forcing and 3 hourly wind forcing) adequately represent both the tides and sea–land breeze influences, the model output is only provided every 6 h and thus underresolves the resulting oceanic processes at time scales shorter than a few days (60 h corresponds to 10 time steps). Hourly model output fields would be needed to study their role in driving transport within Cape Cod Bay. Finally, our current study is limited to the near-surface only, whereas spreading pathways might differ if the potential wastewater was to be released subsurface or subducted along isopycnals by coastal downwelling or other processes. GoMOFS provides vertical velocity data which can be leveraged to calculate trajectories in three dimensions and study transport and spreading pathways away from the surface. Thus, investigating transport in 3D would be a vital and feasible continuation of our research.

Acknowledgments. The authors would like to acknowledge helpful input from Jim Manning (NOAA Northeast Fisheries, retired) and Ken Buesseler (WHOI). We thank the CO-OPS Webmaster for assistance when the NCEI site could not be accessed. We also thank the anonymous reviewers for their suggestions which helped to improve this manuscript. Rypina, Yoshida, and Macdonald received partial support from the National Science Foundation Grant OCE-1923387 and NOAA Sea Grant NA22OAR4170122. Gregory acknowledges graduate student support from the National Science Foundation Grant OCE-2124210. Rypina

would also like to acknowledge partial support from the National Science Foundation Grant OCE-2124210.

Data availability statement. The Gulf of Maine Operational Forecast System (GoMOFS) data used in this paper are available at https://www.ncei.noaa.gov/thredds/catalog/model-gomofs-files/catalog.html. The drifter data from Drifter Tracks from the NE US Shelf and Beyond are available at https://comet.nefsc.noaa.gov/erddap/tabledap/drifters.html.

APPENDIX A

Variable versus Fixed Time-Step Integration Methods

Figure A1 compares trajectories calculated using a variable time scheme with two choices of tolerance and trajectories calculated using a fixed time-step integration scheme with four choices of time step. Trajectory computed with the smallest time step (0.1 h) is nearly indistinguishable from that computed using a variable time scheme with 10^{-9} tolerance values. Also, decreasing tolerance values further does not lead to any changes in the resulting trajectories.

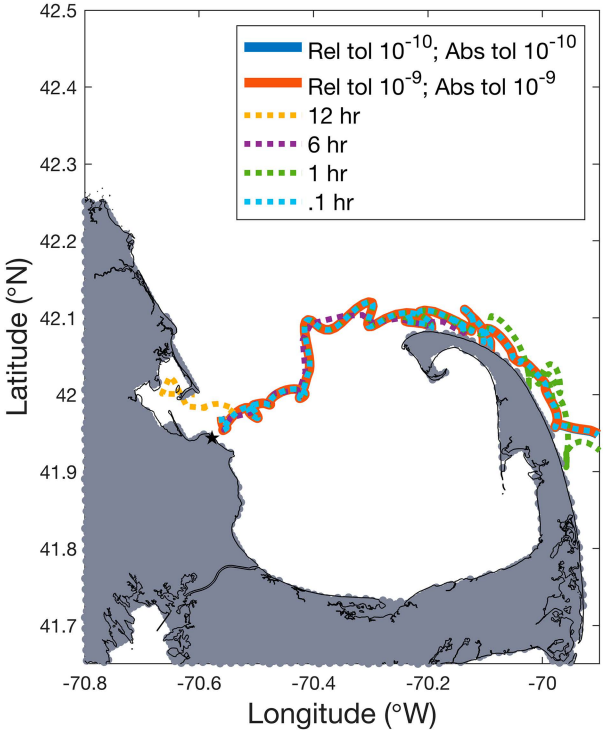

FIG. A1. Comparison between trajectories calculated using a variable time-step scheme (solid lines) and trajectories calculated using prescribed fixed time step (dashed lines).

APPENDIX B

Average Distributions after 60 Days

Figure B1 depicts the average distribution of simulated particles after 60 days. Bright yellow indicates probable final locations, while dark blue indicates improbable final positions. White regions do not contain any particles after 60 days. Bins of high probability line the coasts within the bay, reflecting the large percentage of particles that come into contact with land. Outside of the bay, a line of relatively high probability is observed along the eastern boundary of our domain, suggesting that a large percentage of particles that exit the bay are transported out of our domain and into the Atlantic after 60 days. Within the bay, probabilities are generally low, suggesting that while some particles are still circulating within the bay after 60 days, their percentage is small compared to particles that end up on land or out of the domain. Winter 2020 and summer 2019 have the most particles still circulating after 60 days. However, even during those two seasons, the percentage is still low (7% and 5%, respectively) compared to the percentage of particles that end up on land or out of the bay (93% and 95%, respectively).

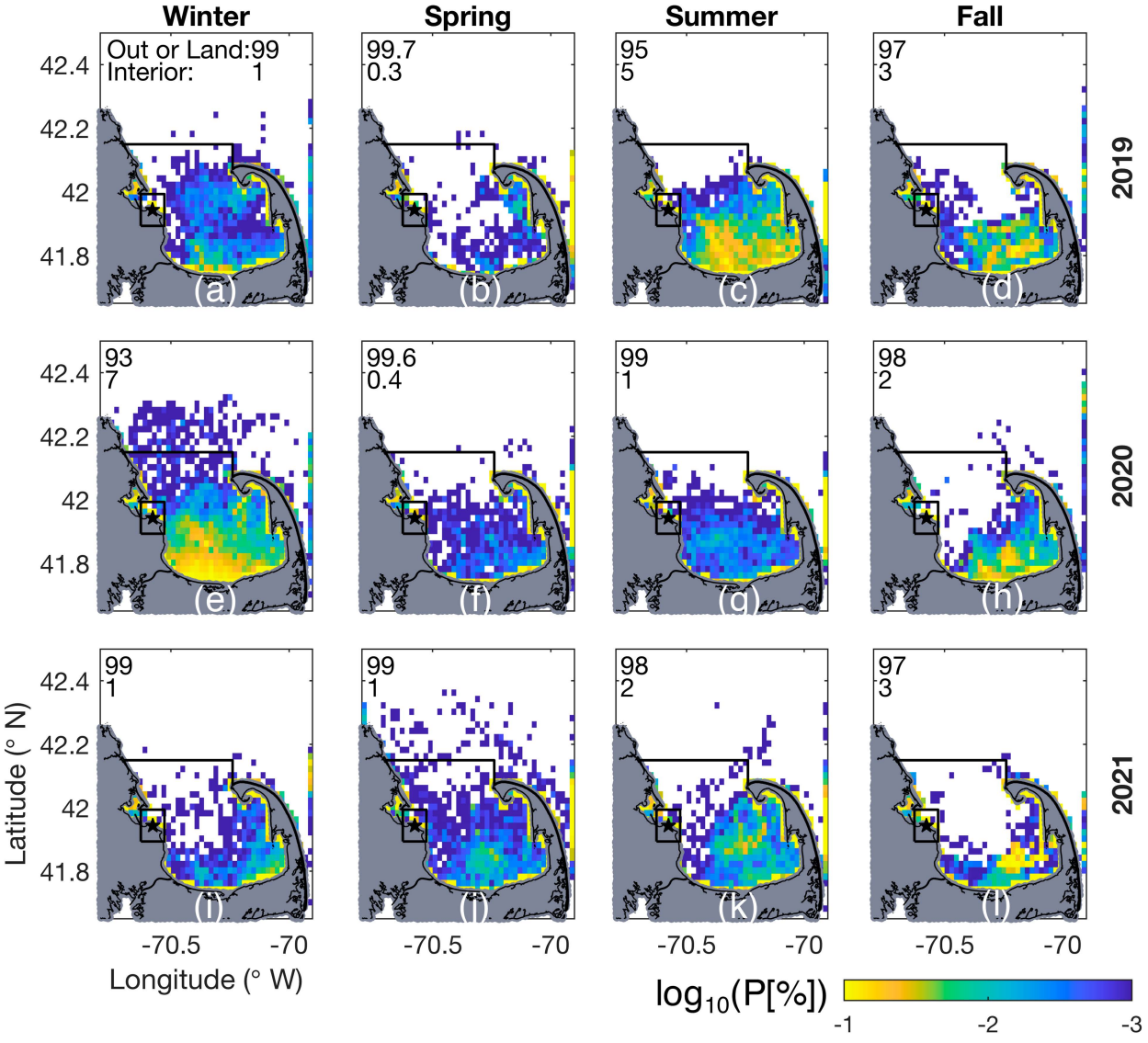

FIG. B1. Average distribution (log scale for visibility) of released particles after 60 days. Numbers report the percentage of simulated particles that have final positions out of the bay or on land and the percentage still circulating within the bay.

APPENDIX C

Definition of Out of the Bay

Here, we investigate the sensitivity (or the lack of such) of our transport characteristics to the exact choice of the boundary of the bay. In section 2d, a meridional line at 42.15°N is used to define out of the bay when calculating residence times. This choice is motivated by the existence of simulated particles that meander slightly north and south while being advected eastward toward Race Point. The exact placement of that meridional boundary, however, has only a minor effect on our results. In fact, omitting the meridional line and defining out of the bay as a region to the north and east of Race Point result in only slightly longer residence times (as seen in Fig. C1) and virtually the same average number of particles exiting the bay in each season (as seen in Fig. C2).

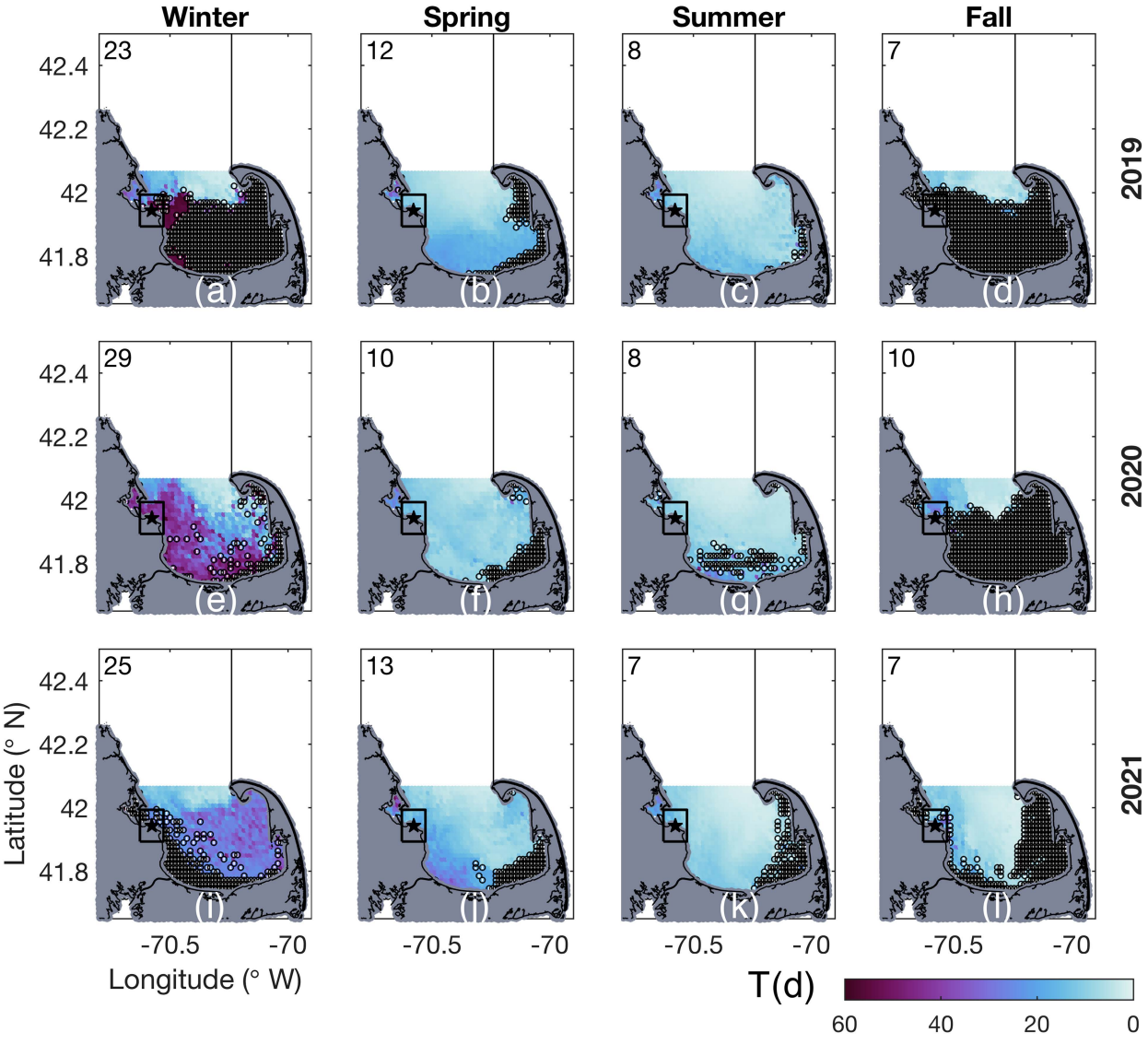

FIG. C1. As in Fig. 12, but with a different choice of the domain boundary.

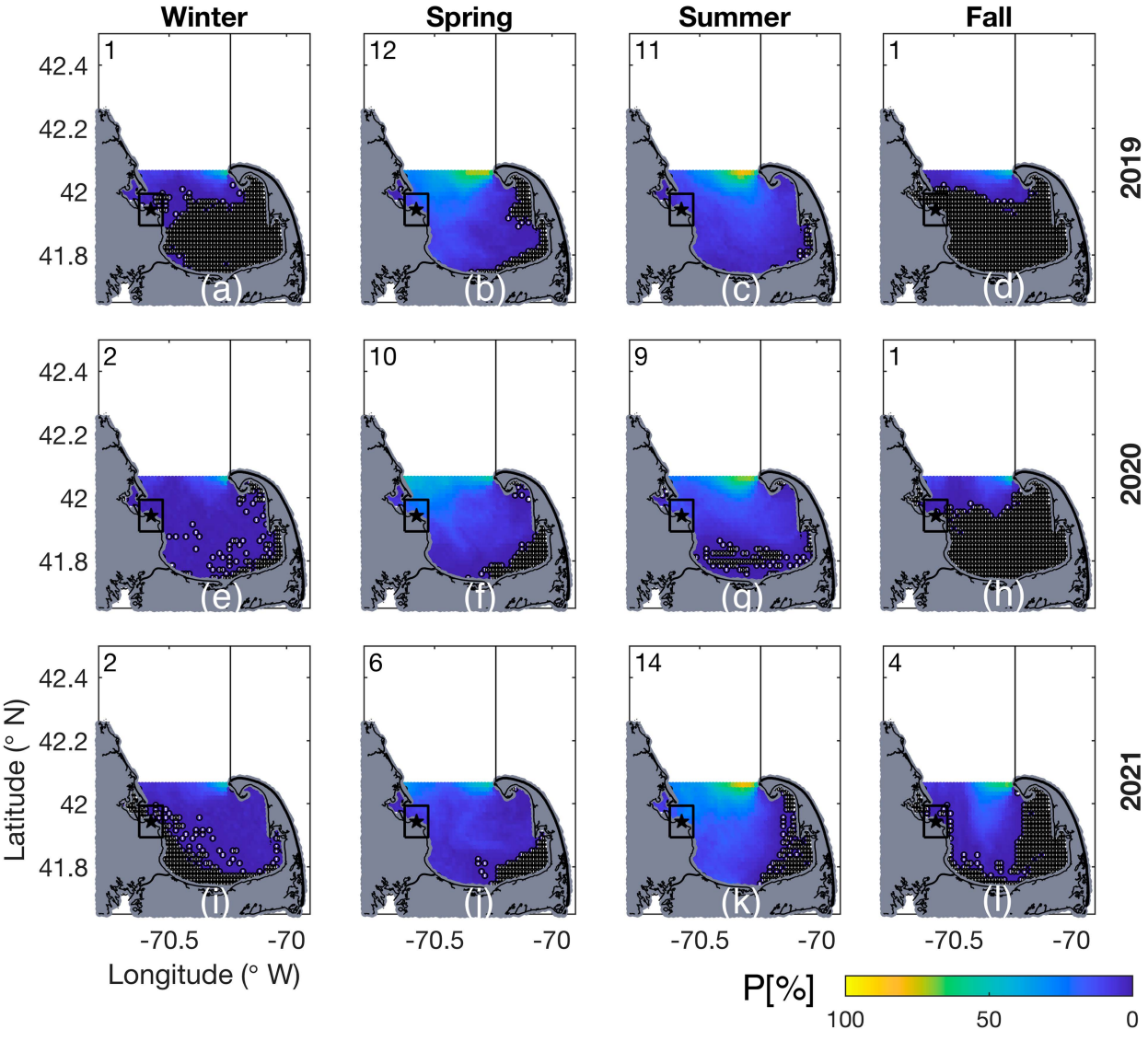

FIG. C2. As in Fig. 13, but with a different choice of the domain boundary.

APPENDIX D

Effects of Wind-Driven Circulation on the Residence Times

A similar analysis to that described in section 3c is carried out for the residence time maps, this time averaging the Ekman currents over 60 days (instead of 3 weeks) and separating the trajectories into six categories according to Ekman current direction (the purple and gray sectors in Fig. D1) and magnitude: *weak* (the bottom 25%), *medium* (between 25% and 75%), and *strong* (the top 25%) documented in Table D1. Here, the gray sector encompasses eastward/east-southeastward Ekman currents, while the purple sector includes southwestward Ekman currents. As in section 3c, a correlation is drawn between winter and fall and predominantly south/southwestward Ekman currents and between predominantly eastward Ekman currents and the spring and summer seasons.

The resulting residence time maps and corresponding percentage of particles that exit the bay are plotted in Figs. D2 and D3, respectively. During times dominated by southwestward Ekman currents, only particles released near the mouth of the bay are able to exit. On the other hand, predominantly eastward Ekman currents enable particles released throughout the entire bay, except for Wellfleet Harbor, to exit the bay. These patterns match the observed seasonality in Fig. 13, with a greater number of particles with initial positions away from the mouth of the bay exiting when released during spring and summer as compared to winter and fall.

However, due to the differences in the spatial and temporal structures of the Ekman currents and the full currents, trajectories estimated using the full currents versus just the Ekman currents are often distinctly different. A representative example in which 1500 particles were released across

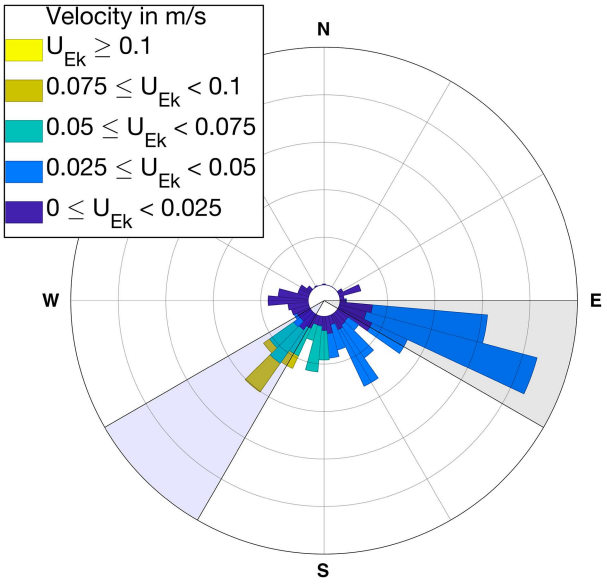

FIG. D1. Ekman currents from 2019 to 2021 after performing a 60-day running average. Two lobes are outlined: Ekman currents flowing to the east lying in the gray sector and southwestward Ekman currents centered in the light purple sector.

TABLE D1. First and third quartile values for the 60-day running averaged Ekman currents at 1 m below the surface, separated by year. Strong Ekman currents correspond to values above the third quartile, weak Ekman currents are values below the first quartile, and medium Ekman currents lie between the two limits.

Year	First quartile (m s^{-1})	Third quartile (m s^{-1})
2019	0.0153	0.0458
2020	0.0195	0.0585
2021	0.0210	0.0630

the bay on 0000 UTC 26 April 2019 is seen in Fig. D4. Averaged over the 3-week integration period, the Ekman currents (Fig. D4b) are nearly spatially uniform in magnitude and direction due to the large scale of atmospheric processes, while the full currents (Fig. D4a) display small-scale spatial variability. The trajectories in Fig. D4c are advected by the full currents to the east and have final positions near Race Point and the Outer Cape, while the majority of trajectories in Fig. D4d are pushed north by the Ekman currents. As a result of these differences, we conclude that Ekman currents alone cannot predict the spread of a potential wastewater plume.

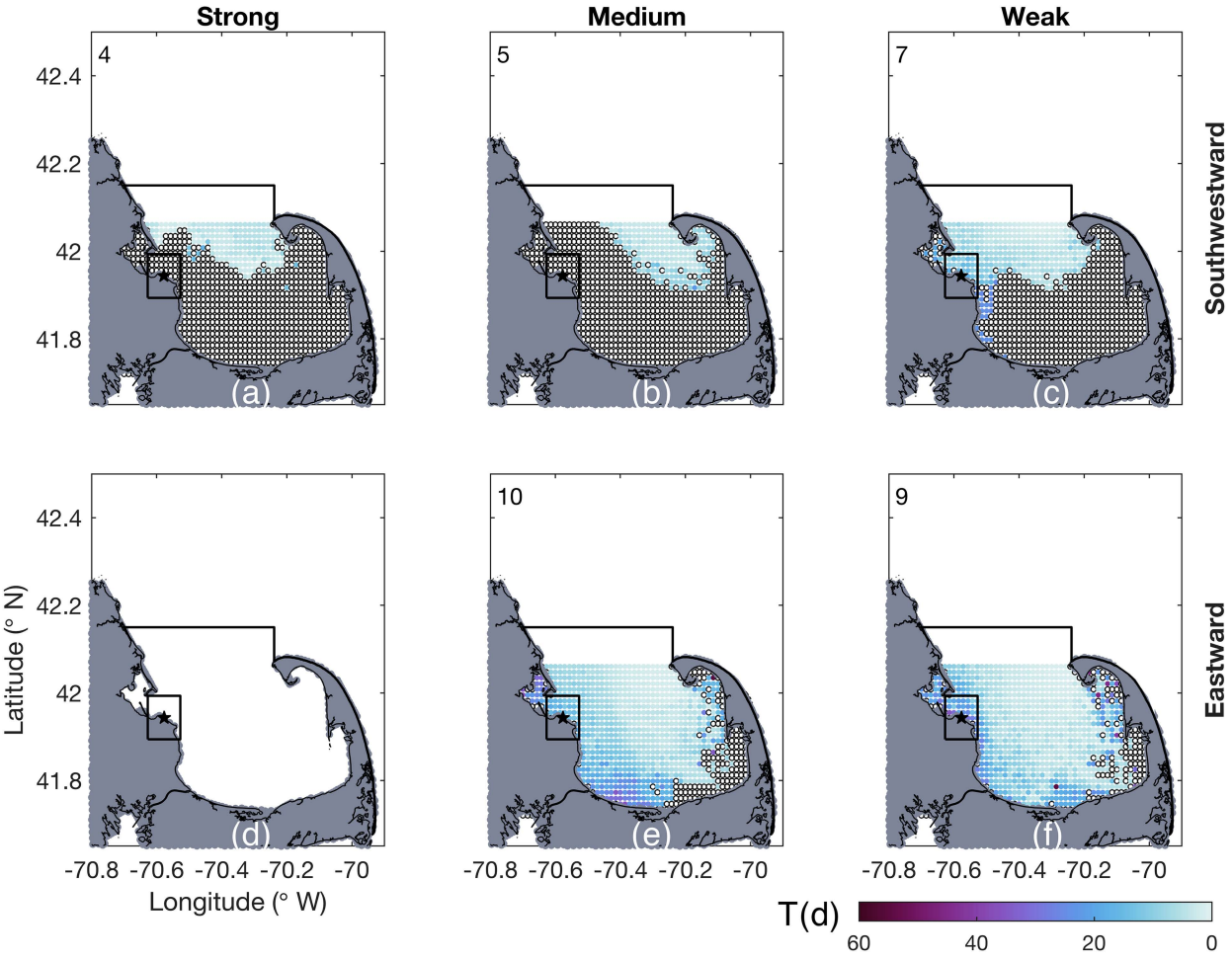

FIG. D2. (a)–(f) Average residence time, separated by dominant Ekman current, in days for release locations located across the full bay. Black circles indicate locations from which no particles exited the bay after 60 days. Numbers in the upper-left corner indicate the domain-averaged residence times in days. There is no color in (d) since zero particles experience strong, eastward Ekman currents on average over the integration period.

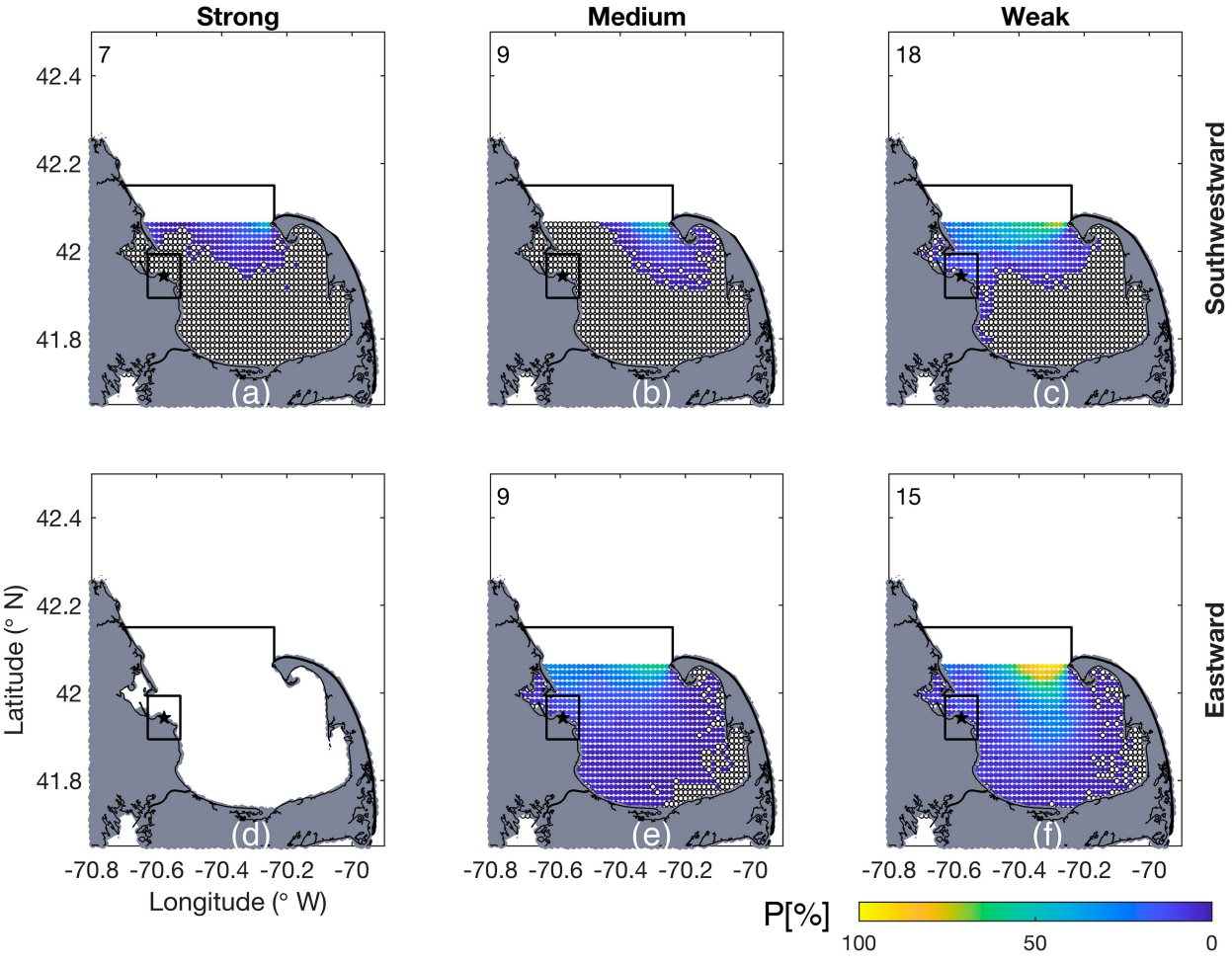

FIG. D3. Average probability of a particle exiting the bay, separated by dominant Ekman current, for each release location. Black circles indicate regions from which no particles exited the bay after 60 days. Numbers report the domain-averaged percentage of particles that exit the bay within 60 days.

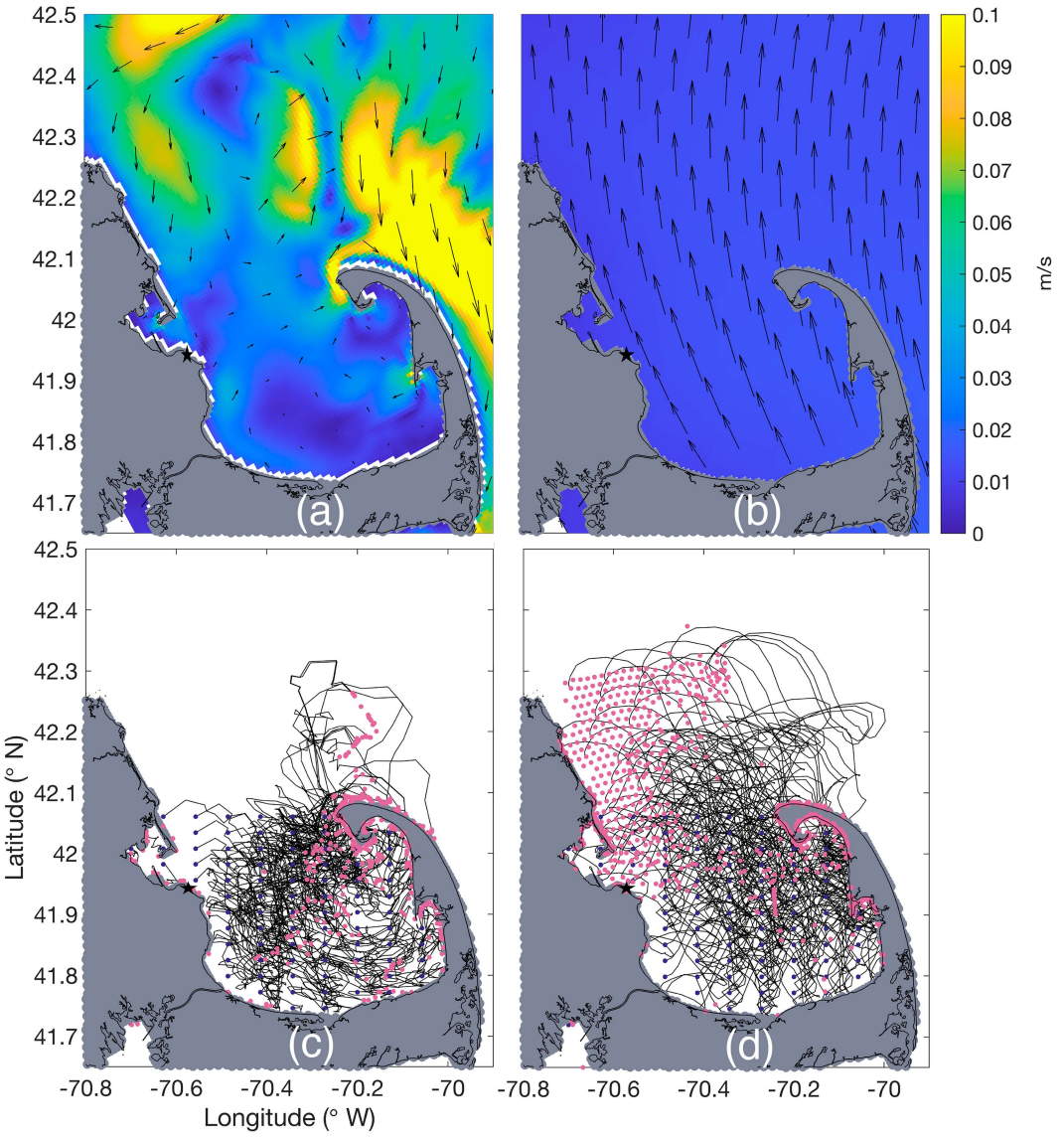

FIG. D4. Sample release comparing trajectories calculated using the full model velocities versus just the calculated Ekman currents. (a) Mean surface currents over 3-week period corresponding to the particle's integration. (b) Mean Ekman currents at 1 m below the surface over the same period. (c) Trajectories estimated from full currents. (d) Trajectories estimated from the Ekman currents. Black lines in (c) and (d) denote a subset of the calculated trajectories, with blue dots in their initial positions. Pink dots denote the final positions of all released particles.

REFERENCES

Beşiktepe, Ş. T., P. F. J. Lermusiaux, and A. R. Robinson, 2003: Coupled physical and biogeochemical data-driven simulations of Massachusetts Bay in late summer: Real-time and post-cruise data assimilation. *J. Mar. Syst.*, **40**, 171–212, https://doi.org/10.1016/S0924-7963(03)00018-6.

Brink, K. H., 2023: *Physical Oceanography of Continental Shelves*. Princeton University Press, 272 pp.

Buesseler, K. O., 2020: Opening the floodgates at Fukushima. *Science*, **369**, 621–622, https://doi.org/10.1126/science.abc1507.

Davis, R. E., 1985a: Drifter observations of coastal surface currents during CODE: The method and descriptive view. *J. Geophys. Res.*, **90**, 4741–4755, https://doi.org/10.1029/JC090iC03p04741.

——, 1985b: Drifter observations of coastal surface currents during CODE: The statistical and dynamical views. *J. Geophys. Res.*, **90**, 4756–4772, https://doi.org/10.1029/JC090iC03p04756.

Fraser, D., 2022: Alternatives sought to dumping of contaminated water into Cape Cod Bay. *Cape Cod Times*, 15 January, https://capecodtimes.com/story/news/2022/01/15/alternatives-dumping-radioactive-water-cape-cod-bay-urged-ma-pilgrim/6515136001/.

Geyer, W. R., G. B. Gardner, W. S. Brown, J. D. Irish, B. Butman, T. C. Loder, and R. P. Signell, 1992: Physical oceanographic investigation of Massachusetts and Cape Cod Bays. USGS Tech. Rep., 23 pp., https://pubs.usgs.gov/publication/70196621.

Gille, S. T., S. G. Llewellyn Smith, and N. M. Statom, 2005: Global observations of the land breeze. *Geophys. Res. Lett.*, **32**, L05605, https://doi.org/10.1029/2004GL022139.

Holtec International, 2022: Information sheet for pilgrim station stakeholders. Holtec International, 6 pp., https://holtecinternational.com/wp-content/uploads/2022/01/Info-Sheet-for-Stakeholder-Water-Disposal-Final.pdf.

——, 2023: Pilgrim Decommissioning. Holtec International, accessed 6 November 2023, https://holtecinternational.com/company/divisions/hdi/our-fleet/pilgrim/.

Jiang, M., M. W. Brown, J. T. Turner, R. D. Kenney, C. A. Mayo, Z. Zhang, and M. Zhou, 2007: Springtime transport and retention of *Calanus finmarchicus* in Massachusetts and Cape Cod Bays, USA, and implications for right whale foraging. *Mar. Ecol. Prog. Ser.*, **349**, 183–197, https://doi.org/10.3354/meps07088.

Kosovsky, L., 2022: The chemical characterization of microplastic polymer composition from various littoral environments on Cape Cod, Massachusetts. Chemistry Honors Papers, 103 pp., https://digitalcommons.conncoll.edu/chemhp/32.

Lermusiaux, P. F. J., 2001: Evolving the subspace of the three-dimensional multiscale ocean variability: Massachusetts Bay. *J. Mar. Syst.*, **29**, 385–422, https://doi.org/10.1016/S0924-7963(01)00025-2.

——, and Coauthors, 2019: Plastic pollution in the coastal oceans: Characterization and modeling. *OCEANS 2019 MTS/IEEE SEATTLE*, Seattle, WA, Institute of Electrical and Electronics Engineers, 1–10, https://doi.org/10.23919/OCEANS40490.2019.8962786.

Liu, X., J. Manning, R. Prescott, F. Page, H. Zou, and M. Faherty, 2019: On simulating cold-stunned sea turtle strandings on Cape Cod, Massachusetts. *PLOS ONE*, **14**, e0204717, https://doi.org/10.1371/journal.pone.0204717.

McGillicuddy, D. J., and Coauthors, 2014: A red tide of *Alexandrium fundyense* in the Gulf of Maine. *Deep-Sea Res. II*, **103**, 174–184, https://doi.org/10.1016/j.dsr2.2013.05.011.

Miller, S. T. K., B. D. Keim, R. W. Talbot, and H. Mao, 2003: Sea breeze: Structure, forecasting, and impacts. *Rev. Geophys.*, **41**, 1011, https://doi.org/10.1029/2003RG000124.

Mukai, A. Y., J. J. Westerink, and R. A. Luettich, 2002: Guidelines for using Eastcoast 2001 database of tidal constituents within western North Atlantic Ocean, Gulf of Mexico and Caribbean Sea. US Army Corps of Engineers Tech. Rep. ERDC/CHL CHETN-IV-40, 20 pp., https://coast.nd.edu/reports_papers/chetn-iv-40.pdf.

Peng, M., A. Zhang, and Z. Yang, 2018: Implementation of the Gulf of Maine Operational Forecast System (GOMOFS) and the semioperational nowcast/forecast skill assessment. NOAA Tech. Rep. NOS CO-OPS 88, 75 pp., https://doi.org/10.25923/am8y-yk96.

Pereira, D., 2020: Wind Rose. MATLAB Central File Exchange, accessed 10 January 2023, https://www.mathworks.com/matlabcentral/fileexchange/47248-wind-rose.

Pond, S., and G. L. Pickard, 1983: *Introductory Dynamical Oceanography*. Gulf Professional Publishing, 329 pp.

Price, J. F., and M. A. Sundermeyer, 1999: Stratified Ekman layers. *J. Geophys. Res.*, **104**, 20 467–20 494, https://doi.org/10.1029/1999JC900164.

——, R. A. Weller, and R. Pinkel, 1986: Diurnal cycling: Observations and models of the upper ocean response to diurnal heating, cooling, and wind mixing. *J. Geophys. Res.*, **91**, 8411–8427, https://doi.org/10.1029/JC091iC07p08411.

Robinson, A. R., and P. Lermusiaux, 2001: Data assimilation (physical/interdisciplinary). *Encyclopedia of Ocean Sciences*, J. H. Steele, S. Thorpe, and K. Turekian, Eds., Academic Press, 302–308.

——, and Coauthors, 1999: Realtime forecasting of the multidisciplinary coastal ocean with the Littoral Ocean Observing and Predicting System (LOOPS). *Third Conf. on Coastal Atmospheric and Oceanic Prediction and Processes*, New Orleans, LA, Amer. Meteor. Soc., 2.18, http://mseas.mit.edu/publications/PDF/robinson_loops_1999.pdf.

Rypina, I. I., L. J. Pratt, and M. S. Lozier, 2011: Near-surface transport pathways in the North Atlantic Ocean: Looking for throughput from the subtropical to the subpolar gyre. *J. Phys. Oceanogr.*, **41**, 911–925, https://doi.org/10.1175/2011JPO4498.1.

——, A. R. Kirincich, R. Limeburner, and I. A. Udovydchenkov, 2014: Eulerian and lagrangian correspondence of high-frequency radar and surface drifter data: Effects of radar resolution and flow components. *J. Atmos. Oceanic Technol.*, **31**, 945–966, https://doi.org/10.1175/JTECH-D-13-00146.1.

——, A. Kirincich, and T. Peacock, 2021: Horizontal and vertical spreading of dye in the coastal ocean of the northern Mid-Atlantic bight. *Cont. Shelf Res.*, **230**, 104567, https://doi.org/10.1016/j.csr.2021.104567.

——, A. Macdonald, S. Yoshida, J. P. Manning, M. Gregory, N. Rozen, and K. Buesseler, 2022: Spreading pathways of pilgrim nuclear power station wastewater in and around Cape Cod Bay: Estimates from ocean drifter observations. *J. Environ. Radioact.*, **255**, 107039, https://doi.org/10.1016/j.jenvrad.2022.107039.

Shchepetkin, A. F., and J. C. McWilliams, 2005: The Regional Oceanic Modeling System (ROMS): A split-explicit, free-surface, topography-following-coordinate oceanic model. *Ocean Modell.*, **9**, 347–404, https://doi.org/10.1016/j.ocemod.2004.08.002.

Signell, R. P., and J. H. List, 1997: Effect of wave-enhanced bottom friction on storm-driven circulation in Massachusetts Bay. *J. Waterw. Port Coastal Ocean Eng.*, **123**, 233–239, https://doi.org/10.1061/(ASCE)0733-950X(1997)123:5(233).

Warner, J. C., B. Butman, and P. S. Dalyander, 2008: Storm-driven sediment transport in Massachusetts Bay. *Cont. Shelf Res.*, **28**, 257–282, https://doi.org/10.1016/j.csr.2007.08.008.

Werme, C., and C. D. Hunt, 2005: 2003 outfall monitoring overview. Tech. Rep. ENQUAD 2004-13, 112 pp., https://www.mwra.com/sites/default/files/2023-11/2004-13.pdf.

Yang, Z., P. Richardson, Y. Chen, E. P. Myers, F. Aikman, J. G. W. Kelley, M. Peng, and A. Zhang, 2019: NOAA's Gulf of Maine Operational Forecast System (GOMOFS): Model development and hindcast skil assessment. NOAA Tech. Memo. NOS CS 38, 54 pp., https://doi.org/10.25923/0m2e-xg81.

Zhang, A., and Z. Yang, 2014: Coastal Ocean Modeling Framework on NOAA'S High Performance Computer (COMF-HPC). NOAA Tech. Rep. NOS CO-OPS 69, 87 pp., https://repository.library.noaa.gov/view/noaa/14421/noaa_14421_DS1.pdf.